Chronostratigraphy of blue ice at the Larsen Glacier in Northern Victoria Land, East Antarctica

Giyoon Lee[1], Jinho Ahn[1], Hyeontae Ju[2], Florian Ritterbusch[3], Ikumi Oyabu[4], Songyi Kim[2], Jangil Moon[2], Christo Buizert[7], Sambit Ghosh[1], Kenji Kawamura[4,5,6], Zheng-Tian Lu[3], Sangbum Hong[2], Chang Hee Han[2], Soon Do Hur[2], Wei Jiang[3], and Guo-Min Yang[3]

[1]School of Earth and Environmental Sciences, Seoul National University, Seoul, South Korea
[2]Korea Polar Research Institute, Incheon, South Korea
[3]Hefei National Laboratory for Physical Sciences at the Microscale, CAS Center for Excellence in Quantum Information and Quantum Physics, University of Science and Technology of China, Hefei, China.
[4]National Institute of Polar Research, Tachikawa, Japan
[5]Department of Polar Science, School of Multidisciplinary Sciences, The Graduate University for Advanced Studies, SOKENDAI, Tachikawa, Japan
[6]Japan Agency for Marine-Earth Science and Technology (JAMSTEC), Yokosuka, Japan
[7]College of Earth, Ocean and Atmospheric Sciences, Oregon State University (OSU), Corvallis, OR, USA

Correspondence to: Jinho Ahn (jinhoahn@gmail.com)

Abstract. Blue ice areas (BIAs) allow for the collection of large-sized old ice samples in a cost-effective way because deep ice outcrops and make old ice samples available close to the surface. However, most chronostratigraphy studies on blue ice are complicated due to fold and fault structures. Here, we report a simple stratigraphy of ice from the Larsen BIA, Antarctica, making the area valuable for paleoclimate studies. Ice layers defined by dust bands and ground penetration radar (GPR) surveys indicate a monotonic increase in age along the ice flow direction on the downstream side, while the upstream ice exhibits a potential repetition of ages on scales of tens of meters, as shown in the complicated fold structure. Stable water isotopes ($\delta^{18}O_{ice}$ and δ^2H_{ice}) and components of the occluded air (i.e., CO_2, N_2O, CH_4, $\delta^{15}N$-N_2, $\delta^{18}O_{atm}$ (= $\delta^{18}O$-O_2), $\delta O_2/N_2$, $\delta Ar/N_2$, ^{81}Kr and ^{85}Kr) were analyzed for surface ice and shallow ice core samples. Correlating $\delta^{18}O_{ice}$, $\delta^{18}O_{atm}$, and CH_4 records of Larsen ice with existing ice core records indicates that the gas age at shallow coring sites ranges between 9.2–23.4 ka BP and ice age for entire surface sampling sites between 5.6–24.7 ka BP. Absolute radiometric ^{81}Kr dating for the two cores confirms the ages within acceptable levels of analytical uncertainty. Our study demonstrates that BIA in northern Victoria Land may help researchers obtain high-quality records for paleoclimate and atmospheric greenhouse gas compositions through the last deglaciation.

1 Introduction

Ice cores serve as very useful archives for paleoclimate records, such as ancient atmospheric greenhouse gas composition, surface temperature, and aerosols. For instance, ice core records reveal the relationship between greenhouse gas concentration and Earth's climate (Petit et al., 1999; EPICA Community Members, 2004; Siegenthaler et al., 2005), abrupt climate changes

during the last glacial period (Dansgaard et al., 1989; Steffensen et al., 2008), and bipolar seesaw climate links on millennium timescales (Blunier and Brook, 2001; Landais et al., 2015). Thus far, continuous climate records from ice cores cover the last

35   800 ka and may reach more than 1 Ma in the near future by new deep drilling projects in Antarctica (Fischer et al., 2013). However, the use of ice cores obtained from conventional deep ice core drilling projects remains limited as many analyses require large amounts of ice, such as trace element isotope and trace gas analyses. In addition, deep drilling projects incur high economic and labour costs. In contrast, coring in blue ice areas (BIAs) has emerged as an alternative to obtain large ice samples in a cost-effective manner (Folco et al., 2006; Petrenko et al., 2006; Schaefer et al., 2006; Sinisalo et al., 2007; Korotkikh et

40   al., 2011; Turney et al., 2013; Bauska et al., 2016; Aarons et al., 2017; Baggenstos et al., 2017; Yan et al., 2019; Fogwill et al., 2020).

In BIAs, old ice is exposed on the surface because the bedrock or basal topographic obstacles cause deep glacial flow upward, and surface snow is ablated by katabatic wind and/or sublimation (Bintanja, 1999; Sinisalo and Moore, 2010). Because ice layers of the same age (isochrones) are extended on the surface, we can obtain large amounts of old ice for a specific age at

45   the surface and/or relatively shallow depths, allowing researchers to study paleoclimate which is typically prohibited by limited sample sizes (Schaefer et al., 2006; Bauska et al., 2016; Fogwill et al., 2020).

In the early stage of BIA research, meteorites were the focus of investigation because ice flow and ablation cause meteorites to accumulate on the surface of the blue ice (Whillans and Cassidy, 1983; Cassidy et al., 1992, Harvey, 2003). Recently, studies on BIAs have drawn attention to the possibility of identifying ice older than 800 ka because glacial–interglacial cycles changed

50   from 40 to 100 kyr during the 0.8–1.0 Ma period, which is called the mid-Pleistocene Transition (MPT). It has been reported that ice at Allan Hills BIA has ages of 90–250 ka on the surface (Spaulding et al., 2013), reaching ~2.7 Ma near the bedrock at depths of about 150–200 m (Yan et al., 2019). However, the use of blue ice has several drawbacks. In most cases, the stratigraphy of the blue ice is complicated, as shown by the fold and fault structures on the surface (Folco et al., 2006; Petrenko et al., 2006; Curzio et al., 2008; Schaefer et al., 2009; Baggenstos et al., 2017) and stratigraphy is discontinuous at deep depths

55   near the bedrock where ice ages are similar to or older than the MPT (Higgins et al., 2015; Yan et al., 2019).

Generally, because of the complicate stratigraphy, blue ice is dated using multiple methods (Sinisalo and Moore, 2010). In previous studies, ice flow modelling, correlation analysis with stable isotopes of ice, and radiometric analysis of meteorites and tephra in ice were used, but the age constraints have not been sufficiently precise to study paleoclimate (Azuma et al., 1985; Nakawo et al., 1988; Reeh et al., 2002; Folco et al., 2006; Aciego et al., 2007; Curzio et al., 2008; Dunbar et al., 2008).

60   A successful method for dating blue ice is to correlate globally well-mixed atmospheric gas records (e.g., CH_4, CO_2, $\delta^{18}O_{atm}$) and glaciochemical records (e.g., nss-Ca^{2+}, $\delta^{18}O_{ice}$, δ^2H_{ice}) with existing well-dated ice core records (Spaulding et al., 2013; Baggenstos et al., 2017; Baggenstos et al., 2018; Menking et al., 2019). Other effective methods include the use of stable Ar isotopes (Higgins et al., 2015; Yau et al., 2015; Yan et al., 2019) or the radioactive ^{81}Kr (Loosli&Oeschger 1969; Buizert et al., 2014; Tian et al., 2019; Crotti et al., 2021), which both provide independent and absolute age constraints.

65   CH_4 and O_2 are well-mixed in the atmosphere (Blunier et al., 2007), and conducting correlations of both CH_4 concentration and $\delta^{18}O$ of O_2 ($\delta^{18}O_{atm}$) is a well-known strategy for establishing chronologies of blue ice (Petrenko et al., 2006; Baggenstos

et al., 2017). Variations in continental ice mass are known to be the main factor that controls $\delta^{18}O_{atm}$ during glacial−interglacial cycles (Bender et al., 1985; Sowers et al., 1993). In addition, variations in the Inter Tropical Convergence Zone (ITCZ) were also considered controlling $\delta^{18}O_{atm}$ on millennial and orbital timescales (Severinghaus et al., 2009; Landais et al., 2010; Seltzer

70   et al., 2017; Extier et al., 2018b). Because of the long lifetime of oxygen gas in the atmosphere (~1 ka), the $\delta^{18}O_{atm}$ varies more gradually, limiting synchronization to millennial timescales. In contrast, atmospheric CH_4 concentration changes rapidly because of the short lifetime of ~12 years, allowing precise dating via stratigraphic matching. Oeschger (1987) suggested the potential of ^{81}Kr measurements in ice core dating. However, at that time, 10^5–10^6 kg of ice was required. In virtue of developing Atom Trace Trap Analysis (ATTA), the required ice has kept decreasing (Lu et al., 2014; Tian et al 2019; Jiang et al., 2020;

75   Crotti et al., 2021). Buizert et al. (2014) for the first time, showed that ^{81}Kr age dating is feasible for blue ice in Taylor Glacier, Antarctica.

BIAs cover 1.67 % of the area of the Antarctic continent and are concentrated in Victoria Land, the Transantarctic Mountains, Dronning Maud Land and the Lambert Glacier basin (Hui et al., 2014) (Fig. 1). Several chronological studies of BIAs in Antarctica have been conducted in Southern Victoria Land: Taylor Glacier (Aciego et al., 2007; Buizert et al., 2014;

80   Baggenstos et al., 2017; Baggenstos et al., 2018; Menking et al., 2019), Allan Hills (Spaulding et al., 2013; Higgins et al., 2015; Yan et al., 2019), Mullins Glacier (Yau et al., 2015); and Northern Victoria Land: Frontier Glacier (Folco et al., 2006; Curzio et al., 2008; Welten et al., 2008). Studies on the Taylor Glacier and Allan Hills BIA have constrained the age of the blue ice along several transects and cores. However, chronologies of the other BIAs in Victoria Land remain insufficient for high-resolution paleoclimate studies. In addition, important paleoclimate proxies such as stable water isotopes, greenhouse gas

85   concentrations, and isotopic ratio of the oxygen gas are not previously addressed for the area.
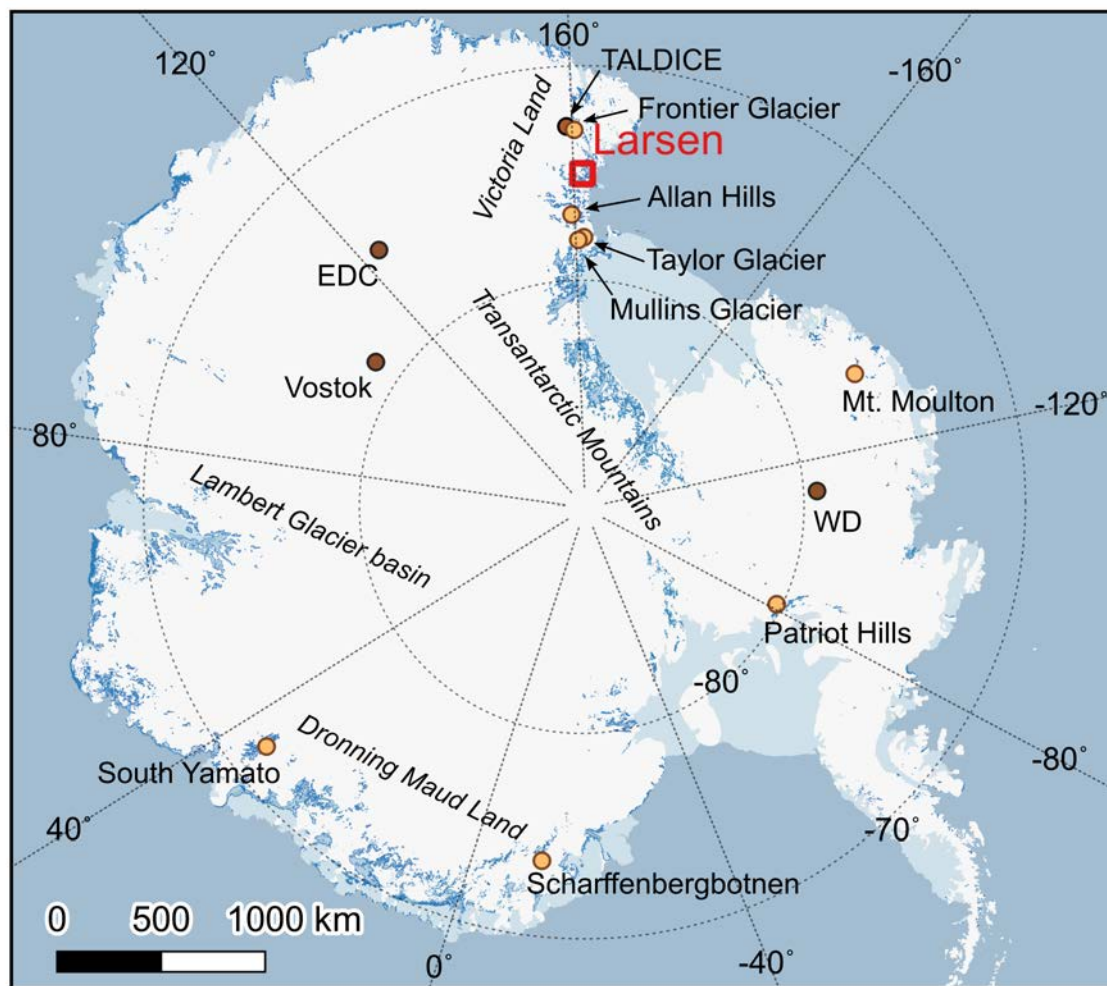
Figure 1. Distribution map of BIAs in Antarctica. BIAs are noted in dark blue (Hui et al., 2014). Orange dots represent the BIAs where the chronology has been studied. Deep ice core locations with brown dots are labeled as follows: Talos Dome ice core (TALDICE), EPICA Dome C (EDC), WAIS Divide (WD) and Vostok. The Antarctic map was obtained from the QGIS Quantarctica package.

90   Our study focused on the chronostratigraphy of ice in Larsen BIA, Antarctica, which may facilitate future research in the region. We describe the ice flow and structure of the ice body using dust bands and ground penetration radar (GPR) surveys, and constrained the unknown gas and ice ages by correlating $\delta^{18}O_{atm}$, CH_4, and $\delta^{18}O_{ice}$ with existing ice core records. We also independently confirmed the ages using the radiometric ^{81}Kr dating method.

2 Study area and methods

95 ### 2.1 Larsen blue ice area (BIA)

We sampled ice from Larsen BIA, an outlet glacier in the Northern Victoria Land, East Antarctica, in austral summer of 2018/2019. The Larsen BIA is located approximately 85 km southwest of the Korean Jang Bo Go station (Fig. 2). The mean annual temperature is −27.2 °C (data and information were obtained from the Meteo-Climatological Observatory at MZS and Victoria Land of PNRA-www.climantartide.it), cold enough to prohibit ice melting in the summer. There were ~20 cm wide

100 dust bands with gentle folding structures in the mid- to downstream part, while we observed severely folded dust bands (e.g. S- and Z-folds) in the upstream part (Fig. 2b). Dust bands are frequently observed in BIAs in Victoria Land and can be used as isochrons (Sinisalo and Moore, 2010). To obtain ice samples with simple stratigraphy, we avoided ice coring in the area with complicated fold structures and sampled ice in the direction of ice flow identified by the Antarctic ice velocity map in QGIS Quantarctica package (Rignot et al., 2011; Mouginot et al., 2012). However, the stratigraphy of the upstream ice, where

105 we collected surface ice may be inverted and repeated on a scale of tens of meters. Shallow ice cores were drilled along a 1 km long transect at intervals of 20–30 m (Fig. 2b). Most ice cores had lengths of approximately 2 m, but ice core #23 (74.9319° S, 161.6018° E) was ~10.4 m (Fig. 2c). We also collected near-surface ice samples (~500 g) along a 1.3 km transect with 20 m intervals to measure stable water isotopes of the ice ($\delta^{18}O_{ice}$, $\delta^{2}H_{ice}$) at depths of ~5–10 cm (hereafter, regarded as the surface ice sample). The ice core TF (74.93042° S, 161.56975° E) with a length of ~12 m on the upstream side was sampled in 2016

110 for a preliminary study, as described by Jang et al. (2017). To define the horizontal distance, we used an imaginary line parallel to the ice flow direction. A line perpendicular to the imaginary line that crosses each sampling location was used to find the intersection point. Then, each intersection point was used to measure the horizontal distance from the most upstream sampling site (Fig. S1).
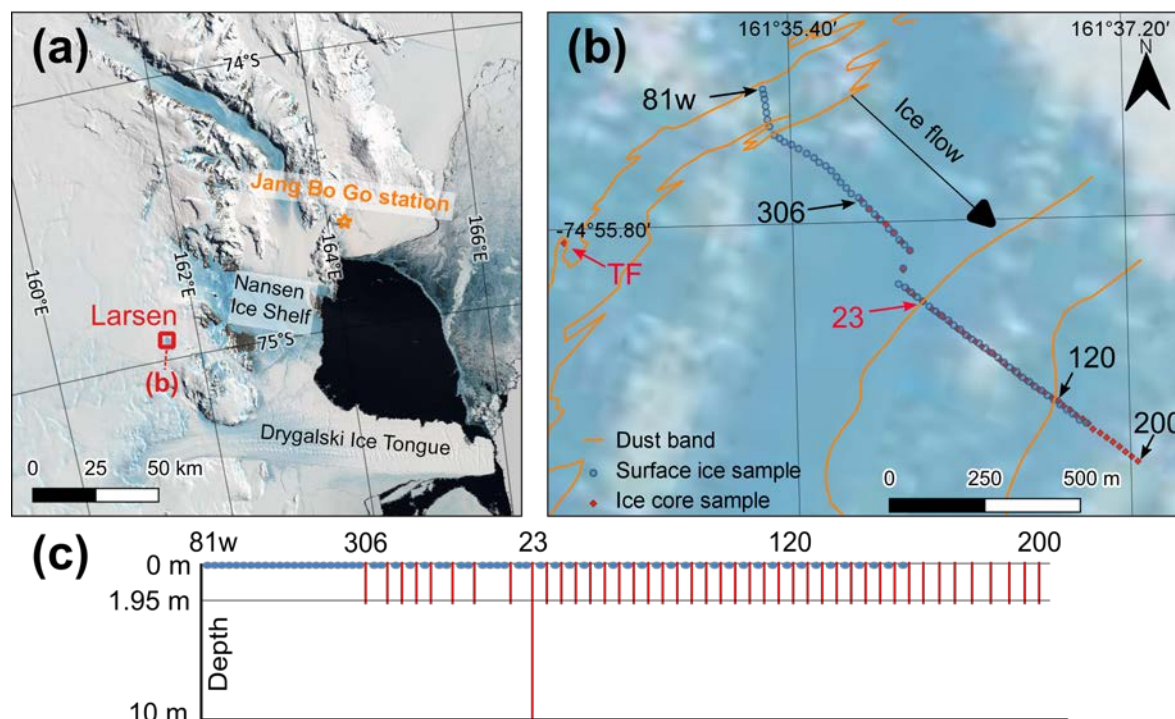
Figure 2. Location of the Larsen BIA and sample collection. (a) Location of Larsen BIA and Jang Bo Go station. **(b)** Magnified map of Larsen BIA including sample locations. Orange lines are dust bands. Blue dots are locations of surface ice samples. Red diamonds are locations of shallow ice cores. Six representative names are shown, red letters for ~10 m long cores (TF and #23), black letters for 2 m long cores (#306, #120 and #200) and surface ice (81W). Z- and S-folds are recognized by the dust bands at upstream ices. The total transect of the ice sample is about 1.4 km. **(c)** Schematized cross-section of the transect. Satellite photo of Antarctica is from the QGIS Quantarctica package (Bindschadler et al., 2008).

2.2 Ground penetrating radar (GPR) survey

Approximately 17 km of GPR data were collected for two days in January 2019 (Fig. S1). A MALÅ ProEx impulse radar system with a 50 MHz unshielded antenna for a larger penetration depth was used for data acquisition. Records were taken at a sampling frequency of 559.5 MHz, time interval 0.1 s and stacked 4 times. The survey was conducted at a speed of 2.5–3 km h^{-1} to minimize noise caused by frictional vibrations between the antenna and the surface of the glacier. The position of traces was recorded using a single-frequency code-phase GPS with an accuracy of < 3 m. Data processing was performed in ReflexW v.9.5 in the order of dewow, DC filter, band-pass filter, time-zero drift, energy decay correction, background removal, static correction, migration, and stack. As the constant radar signal velocity "v" in the glacier was 0.17 m ns^{-1} (Borgorodsky, 1985; Reynolds, 1985), and the frequency "f" of the radar system was 50 MHz, the GPR wavelength "λ" was about 3.4 m (λ = v f^{-1}).

2.3 Stable water isotope measurement

Stable water isotopes ($\delta^{18}O_{ice}$, δ^2H_{ice}) were measured simultaneously at the Korea Polar Research Institute (KOPRI) using the Cavity Ring-Down Spectroscopy (CRDS) method using a Picarro L2130-i with a vaporizer (A0211). Surface ice samples (~5–10 cm depth) and ice core samples (10–30 cm and 190–200 cm depths of ice cores) were used for the analyses. The
135 average horizontal interval of the surface ice samples and ice cores was approximately 10.3 m. Ice from the ~10 m long core #23 was used for measurements at 20 cm intervals. Ice samples were kept in Whirl-Pak and melted at room temperature. The melted sample was then injected into a 2 ml vial via a disposable syringe with a 0.45 μm filter. One batch of measurements consisted of five duplicate samples (10 samples in total) and a working standard. The first and second aliquots of the sample were measured 12 times each, and the working standard was measured 20 times. To remove the memory effects from the
140 previous samples, the last six measurements were used. The precision was evaluated by measuring the working standard repeatedly (n = 67); 1 sigma (standard deviation) was 0.07 ‰ for $\delta^{18}O_{ice}$ and 0.90 ‰ for δ^2H_{ice}. The working standards and samples were calibrated against the international standards for water isotopes, VSMOW2 (Vienna Standard Mean Ocean Water 2), SLAP2 (Standard Light Antarctic Precipitation 2) and GISP (Greenland Ice Sheet Precipitation).

2.4 Greenhouse gas (GHG) measurement

145 The CH_4 concentrations in ice cores (#306, #23, #120, and #201) were analyzed at Seoul National University (SNU) using a melt–refreeze technique with a flame ionization detector gas chromatograph (FID-GC) at 10 cm intervals. The process of CH_4 measurement was described in detail by Yang (2019). Briefly, we trimmed the outermost side and the cracks of the ice samples by approximately 2 mm with a clean band saw to eliminate contamination by ambient air. The mass of the ice used for measurement was about 35–55 g. Then, we placed the ice inside a custom-made flask and evacuated the flask. We used a
150 740.6 ppb standard air sample from the National Oceanic and Atmospheric Administration (NOAA) Global Monitoring Division (GMD) on the WMO X2004A scale to establish a daily calibration line (Dlugokencky et al., 2005). The NOAA standard air was injected into four flasks containing bubble-free ice samples, which served as the control group. The CH_4 mixing ratio of the control group was measured, and the average offset to the standard value of 740.6 ppb was assumed to be a systematic error; thus, the average offset (~2–20 ppb) was subtracted from each measurement result. Trapped gas in the ice
155 was liberated by immersing the flask in a hot water, and then refreezed the melt water. In addition, as CH_4 is more soluble than the major air components (N_2, O_2, and Ar), the CH_4 concentration of the 1st extracted air is lower than the original value. Therefore, 2nd gas extraction was conducted to correct the solubility effect.

The same ice cores (#306, #23, #120, and #201) were used for CO_2 measurements. Generally, CO_2 should be measured using a dry extraction system rather than wet extraction because of its high solubility in water and the possibility of CO_2
160 production by carbonate–acid reactions in ice melt (Delmas et al., 1980). Therefore, for our measurement, air was collected using a needle-crusher dry extraction instrument and detected by FID-GC at SNU. The ice was pre-treated in the same manner as that for CH_4, as described above, while the required amount of ice was 15–20 g. We placed the ice in the needle crush

chamber, which was cooled to −35 °C during ice preparation. The CO_2 results could be affected by adsorption and desorption by the instrument and the sample tube (Ahn et al., 2009). Therefore, before crushing the ice, NOAA standard air was released

165 through the chamber and collected into the sample tube. The CO_2 mixing ratio was measured, and the average offset with respect to NOAA standard air was used to subtract the value of the CO_2 result from each ice sample measurement. The CO_2 mixing ratio of the standard air we used for making a daily calibration line was 285.66 ppm or 293.32 ppm, which is from NOAA GMD in WMO X2019 calibration scale (Hall et al., 2021). Trapped air in the ice was collected in a sample tube cooled by a helium closed cycle refrigerator (He-CCR) after crossing the water trap. The entire process and principle are described in

170 detail by Shin (2014).

We also used ice samples from 35 cores at depths of 190–200 cm (hereafter, regarded as horizontal measurement) and ice core #23 to measure CH_4, CO_2, and N_2O concentrations, along with other gas isotopes (see below), by a wet extraction method at the National Institute of Polar Research (NIPR) in Japan. For CO_2 and CH_4, FID-GC was used, and for N_2O, an electron capture detector (ECD) GC was used. To determine the concentrations of CH_4 and CO_2, a calibration line was established

175 using TU-2008 (Tohoku University) scale standard air; for N_2O, the TU-2006 scale standard air was used. More information on the standard air we used (named STD 1, 3, 5) is given by Oyabu et al. (2020). Three standard air and a quadratic calibration line were used to determine GHG concentration in the NIPR, while single standard air and a linear calibration line were used to determine the GHG concentration in SNU. Different calibration scales of standard air (TU and NOAA/WMO) and different calibration methods may contribute to making an inter-laboratory offset of GHG concentrations. CO_2 was measured again at

180 SNU by the dry extraction method at 190–195 cm depth for the horizontal measurement (Table S4). The ice preparation process is briefly explained in Sect. 2.5.

2.5 Analyses of $\delta^{15}N$-N_2, $\delta^{18}O_{atm}$, and $\delta O_2/N_2$

O_2, N_2, and Ar isotopes were measured at NIPR using a dual inlet mass spectrometer (Thermo Fisher Scientific Delta V). The isotope results are valued with respect to the modern atmosphere. As mentioned previously, we measured 35 ice cores at

185 depths of 190–200 cm to evaluate how ancient air compositions change horizontally and also measured gas isotopes using ice core #23 at several depths with a range of 0–10 m to compare with the results from the neighbouring cores at depths of 190–200 cm. Because gas loss fractionation by molecular diffusion during storage could have affected the isotope results (Ikeda-Fukazawa et al., 2005), we trimmed the surface and the cracks of the ice approximately 3–5 mm and then removed some unclear ice surface with a ceramic knife. The weight of the ice was 55–80 g after trimming the surfaces. The ice inside the

190 vessel was evacuated for ~120 min. To extract the gas, each vessel was gradually immersed in a hot water container. Simultaneously, the released air was collected into a sample tube, which was cooled by a He-CCR. After homogenizing the sample tube for a night, the gas was split into two aliquots, one for isotope analysis (1.5 ml) and the other one for greenhouse gas measurement (5 ml). The measurement process is described in more detail by Oyabu et al. (2020).

Obtaining a true $\delta^{18}O$ value in the past atmosphere from ice cores requires gravitational, thermal, and gas loss fractionation

195 corrections. The gravitational factor is proportional to the difference in the mass number between isotopes (Craig et al., 1988;

Severinghaus et al.,1998). Therefore, $\delta^{18}O$ ($^{18}O/^{16}O$) was affected twice as much as $\delta^{15}N$ ($^{15}N/^{14}N$) by gravity. Hence, each gas isotope was gravity-corrected using Eq. (1):

$$\delta^{18}O_{atm} = \delta^{18}O - 2 \times \delta^{15}N \tag{1}$$

In the same principle, $\delta O_2/N_2$ is affected by a factor of 4 than $\delta^{15}N$, thus it was corrected using Eq. (2) and used for assessing

200   the gas loss fractionation:

$$\delta O_2/N_{2,gravcorr} = \delta O_2/N_2 - 4 \times \delta^{15}N \tag{2}$$

Along with the gravitational correction, thermal fractionation should also be considered because temperature gradients in the firn column affect the distribution of the isotopes (Severinghaus et al., 1998; Goujon et al., 2003). Thermal fractionation is typically small in Antarctic ice cores due to the relatively gradual nature of surface climate change. Comparing $\delta^{40}Ar/4$

205   ($^{40}Ar/^{36}Ar$) and $\delta^{15}N$ together allow discrimination of the contribution of thermal and gravity fractionation (Severinghaus et al., 1998). However, for our samples, thermal fractionation could not be considered because ^{36}Ar interfered with the $^{18}O_2$.

$\delta O_2/N_{2,gravcorr}$ of around −30 ‰ indicates that the ice is poorly preserved, and has experienced considerable gas loss either during drilling or storage (Landais et al., 2003). Following Capron et al. (2010), we did not correct for gas loss fractionation in our samples because the $\delta O_2/N_{2,gravcorr}$ values were significantly greater than −30 ‰, except for one measurement for sample

210   #301 (Table S1, S2). We did not use the results of #301 when constraining the gas age using $\delta^{18}O_{atm}$.

2.6 ^{81}Kr dating

For the ^{81}Kr measurement of ice core #23 and TF, 5.3 kg (depth: 711–1040 cm) and 5.4 kg (depth: 798–1192.5 cm) of ice were used, respectively. Air for the ^{81}Kr measurement was extracted at SNU by the instrument provided by the University of Science and Technology of China (USTC). The ice was kept in a tank with an O-ring lid and evacuated using a dry scroll pump

215   with a water trap. Then, the ice was melted by immersing the tank in hot water. The released gas was collected in containers and shipped to USTC for Kr purification and ^{81}Kr analysis using Atom Trap Trace Analysis (ATTA). The extraction procedure was described in detail by Tian et al. (2019), and the principle of ATTA was described by Jiang et al. (2012).

The anthropogenic ^{85}Kr is measured simultaneously with ^{81}Kr to quantify any contamination with modern air. The ice sample details and krypton dating results are reported in Table 1. For both samples, the measured ^{85}Kr activity is below the detection

220   limit, so no correction for contamination with modern air is necessary. For the calculation of the ^{81}Kr-ages, the changes in the past atmospheric ^{81}Kr abundance due to variation of the cosmic ray flux on the Earth (Zappala et al., 2020) are taken into account. The age uncertainty calculation is based on the statistical error of the atom counting.

Table 1. Results of ^{81}Kr and ^{85}Kr analysis. Errors have a 1σ confidence level, whereas upper limits have a 90% confidence level. The ^{81}Kr age is given with the statistic error due to atom counting. The systematic error of the ^{81}Kr age is due to the uncertainty in the half-life of ^{81}Kr
225   (229 ± 11 ka). pMKr = percent modern krypton; dpm cc^{-1} = decay per minute / cubic centimeter STP of Kr. As ^{85}Kr in modern air in Antarctica is around 65 dpm cc^{-1}, the ^{85}Kr of samples indicate that alteration by modern air is negligible.

Sample	Mass (kg)	Depth (cm)	^{85}Kr (dpm cc^{-1})	^{81}Kr (pMKr)	^{81}Kr age (ka)	Systematic error (ka)

| TF | 5.4 | 798–1192.5 | < 1.2 | 93.5 ± 4.7 | 26^{+15}_{-17} | ± 1 |
| #23 | 5.3 | 711–1040 | < 0.7 | 92.4 ± 4.1 | 29^{+14}_{-15} | ± 1 |

2.7 Development of WD2014 timescale for TALDICE

For the TALDICE ice core we use a timescale that is synchronized to the WAIS Divide (WD) WD2014 chronology (Buizert et al., 2015; Sigl et al., 2016) in the following way. The ice age scales are synchronized using volcanic deposits identified in

230 sulfur/sulfate data from the WD and TALDICE cores (Buizert et al., 2018; Severi et al., 2012). Next, the TALDICE gas-age ice-age difference (Δage) is established empirically by matching abrupt changes in atmospheric CH_4 to the WD core; at each match point this provides one discrete Δage constraint. A dynamical firn densification model based on Herron-Langway firn physics (Herron & Langway, 1980) is then used to interpolate between these empirical Δage constraints, in order to obtain a gas age scale for all depths (Buizert et al., 2021).

235 ## 3 Results and discussion

3.1 Ground penetrating radar (GPR) survey

In the GPR survey, we identified ice layers (or isochrones) in the transect parallel to the ice flow direction (Fig. 3). The dips of the ice layers range from 1° to 6° with a decreasing trend from the upstream to the downstream direction. The ice layers of radargram were not clearly visible at a depth of < 10 m because of the direct wave signal. We did not observe any stratigraphic

240 folding structure in the ice layers that made age inversion along the ice flow direction in the mid- to downstream areas. Therefore, we expect monotonic and continuous age changes along the ice flow direction. However, as shown in the dust bands with S- and Z-folds in the upstream area (Fig. 2b), the upstream stratigraphy might be repeated on a scale of tens of meters. The basal topography is well defined from the GPR data, and we observed an ice thickness variation of 200–400 m (Fig. 3b).

The subsurface ice layer in the upstream area (0–800 m from the most upstream side) was not well recognized from the

245 GPR profile (Fig. 3c). It is possible that noise caused by crevasses, cavities, or cracks could obscure the signals. In addition, accurate data acquisition might have been hindered by antenna tremors or low battery power at a severely cold temperature.

(a)

Bedrock (m)

Ice Thickness (m)

(b)

(c)
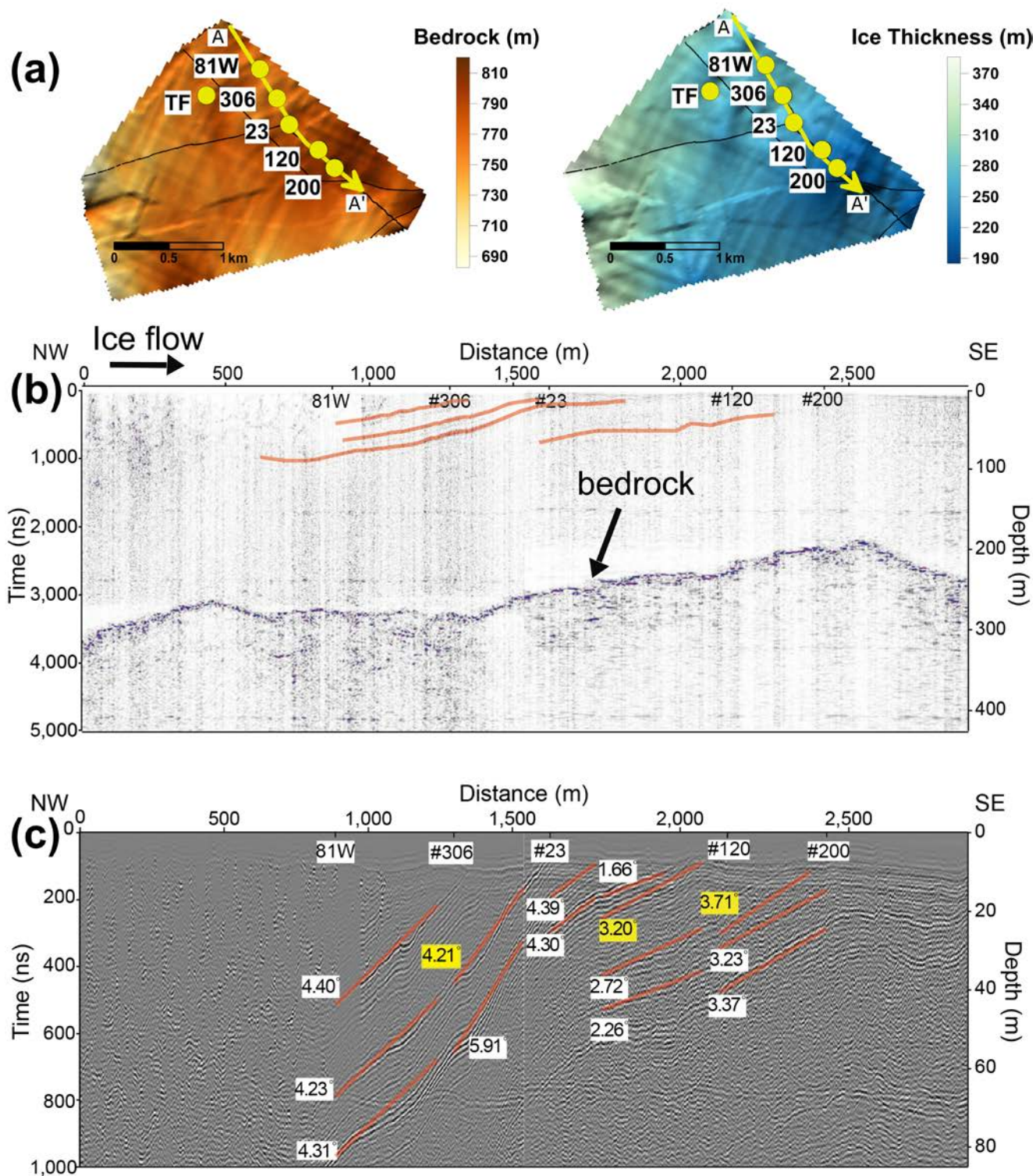
Figure 3. Ground penetrating radar (GPR) survey profile. (a) Bedrock elevation and ice thickness of Larsen BIA. **(b)** GPR profile of the transect (AA′ in (a)) through the blue ice field. Identifiable ice layers are indicated in orange lines. Ice layers are not well identified at a distance of < 800 m. **(c)** Enlarged upper 80 m of the GPR profile. Vertical axis is exaggerated and the dip of the ice ranges 1–6°. The average dip used for estimating the ice ages at 1.95 m depth are shown as yellow boxes (Appendix C).

3.2 Stable water isotopes

Stable water isotopes in ice record surface temperatures in the past at the snow deposition site (Jouzel et al., 1997). The $\delta^{18}O_{ice}$ and δ^2H_{ice} records of Larsen BIA are presented in Table S5, S6, and S7. The horizontal δ^2H_{ice} result has a distinct local minimum around a horizontal distance of 600–800 m, indicating a transient cold event (Fig. 4b). The δ^2H_{ice} of the transient cold event plunges by approximately 70 ‰, heading to the upstream ice. The most downstream sample, ice core #200, has a δ^2H_{ice} of −369 ‰. Conversely, the most upstream sample, surface ice #81W, has a δ^2H_{ice} of −245 ‰. Ice core #23 was located in the middle of the transect, and the vertical δ^2H_{ice} profile shows a range of −353 ‰ to −291 ‰. It appears that the water isotope values from Larsen BIA are more scattered with a wider range than other published ice core records. The highly variable $\delta^{18}O_{ice}$ has also been reported in the Taylor Glacier (Baggenstos et al., 2018; Menking et al., 2019). Severe scattering might indicate that the accumulation zone (original source of ice) of Larsen BIA might have experienced more variability in temperature and/or the vapour source (variability of atmospheric conditions) than other sites.

To match the two δ^2H_{ice} profiles (measurement of ice core #23 and horizontal measurement of near-surface ice), the depth of ice core #23 was converted to the horizontal distances by pinpointing the deepest result of #23 to the result of ice core #104 and conducting linear interpolation. The two δ^2H_{ice} profiles have r^2 value of 0.85 (p < 0.001) (Fig. 4b). The similarity of δ^2H_{ice} between the vertical and horizontal measurements demonstrate that stable water isotopes were not altered while the glacier flowed to the surface and also showed that ice stratigraphy was not disturbed. As the ~10 m long #23 core covers ages that correspond to a surface distance of ~117 m, we calculated the average dip of the ice layer of 4.96°, which is comparable with the average dip derived from the GPR profile (Fig. 3d). This depth/distance relationship is also supported by the comparison of gas isotope values ($\delta^{18}O_{atm}$ and $\delta^{15}N$-N_2) from ice core #23 to the records from the horizontal measurement at a depth of 1.95 m (Fig. A2).
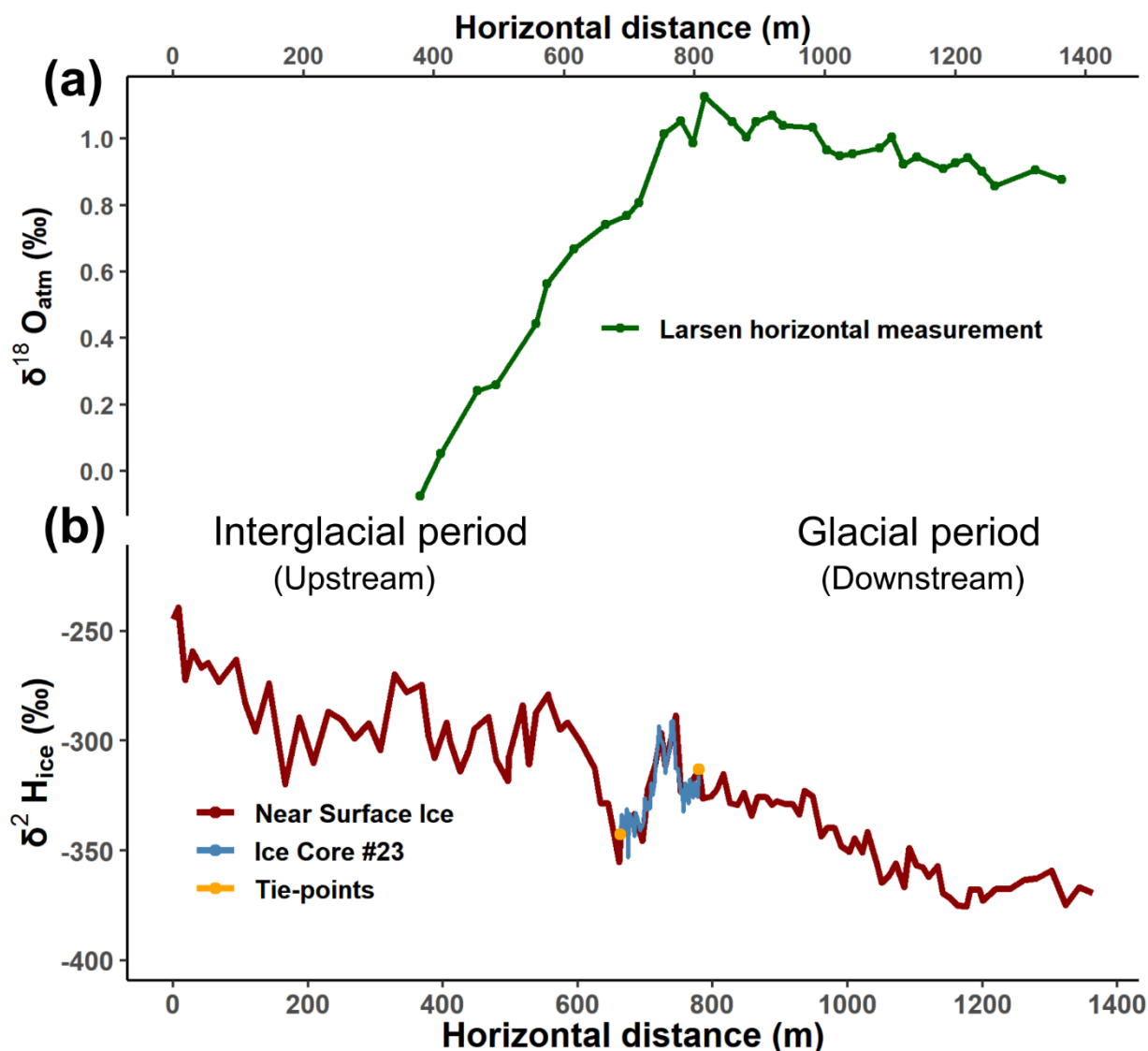
Figure 4. $\delta^{18}O_{atm}$ and δ^2H_{ice} records from Larsen BIA. (a) $\delta^{18}O_{atm}$ from each ice core at a 1.95 m depth (horizontal measurement). The $\delta^{18}O_{atm}$ of the horizontal measurement was gravity-corrected by Eq. (1). (b) δ^2H_{ice} from near-surface ice (~5–10 cm depth surface ice samples and 10–30 cm depth ice core samples) and ice core #23. The surface ice record was matched with core #23 using two tie-points (orange dots) and show a r^2 value of 0.85 ($p < 0.001$).

3.3 CH₄ and CO₂ mixing ratios

The measurement results of CH_4 and CO_2 concentrations for the vertical cores are presented in Fig. A1. The shallow ice cores (#306, #120, #201) show that greenhouse gases are significantly altered for the top 2 m. CH_4 records of #23 also fluctuate significantly at 0–4.6 m depth but settle down at > 4.6 m. CO_2 records of #23, in contrast, gradually decrease and become steady at a depth of > 4.6 m. A comparison of the results from NIPR to SNU with ice core #23 shows that the difference in the

concentration decreases significantly at depths of > 4 m; huge difference (30–140 ppb) of CH_4 at 0–4 m depths, but decreased considerably (5–10 ppb) at a depth of > 4 m; CO_2 difference was 10–20 ppm at < 4 m, but decreased to 2–10 ppm at a depth of > 4 m (Table S2 and S3). Altered CH_4 proximity to the surface is also by reported by Petrenko et al. (2006) and Baggenstos

285 et al. (2017). However, the CO_2 mixing ratio of the TF core, reported by Jang et al. (2017), shows that CO_2 is scattered even in the deeper part of the ice core. We speculate that this scattering of CO_2 can be due to complicated ice stratigraphy because we observed many folding structures identified by dust bands near the TF core site (Fig. 2b).

3.4 $\delta^{15}N$-N_2 and $\delta^{18}O_{atm}$

As N_2 and O_2 are the dominant gas species in atmospheric air, we assumed that the $\delta^{15}N$-N_2 and $\delta^{18}O_{atm}$ were not significantly

290 altered at a depth of 1.95 m. We tested the assumption by comparing the vertical distribution of the ice core #23 with horizontal distribution at depths of 1.95 m in nearby shallow cores. The depths of ice core #23 were converted to horizontal distances at a depth of 1.95 m (Fig. A2) using Eq. (3):

$$\text{Horizontal distance in meter (at 1.95 m depth)} = \{|(\text{depth of ice core \#23}) - 1.95|/\tan(4.96°)\} + 663 \tag{3}$$

We added 663 m because ice core #23 was located 663 m from the most upstream sampling site. The average dip of the ice

295 layer (4.96°) was calculated by matching the δ^2H_{ice} of ice core #23 with the horizontal records from the neighbouring cores. The $\delta^{15}N$-N_2 and $\delta^{18}O_{atm}$ values obtained from the horizontal record at 1.95 m are comparable to those from ice core #23 except those from the very shallow depths of < 0.5 m (Fig. A2), confirming that the gas isotope ratios are generally reliable at a depth of 1.95 m. We estimated the uncertainty of $\delta^{15}N$-N_2 and $\delta^{18}O_{atm}$ values as ±0.05 ‰ because the offsets between #23 and the horizontal record are approximately 0.05 ‰. Petrenko et al. (2006) also reported that as long as the ice is not affected by

300 surface ice melting, nitrogen and oxygen gas isotopes are not altered even at a depth of 0.3 to 0.4 m at the western Greenland ice. No significant gaps, discontinuities, or anomalies were found within the results from horizontal measurements of $\delta^{18}O_{atm}$, which indicate no significant stratigraphic disturbance (Fig. 4a).

3.5 Glacial termination identification in Larsen ice

The increase in δ^2H_{ice} and decrease in $\delta^{18}O_{atm}$ from the downstream to upstream ice shows that the atmospheric conditions

305 changed to a warmer climate (Fig. 4). In particular, the $\delta^{18}O_{atm}$ values of the Larsen ice (1.126 ‰ to −0.075 ‰) reveal a typical glacial termination period. The maximum $\delta^{18}O_{atm}$ value of > 1 ‰ implies that the ice is younger than 800 ka because the glacial climate conditions became more extreme after the MPT (Lisiecki and Raymo, 2005; Elderfield et al., 2012; Chalk et al., 2017); and it is likely that the maximum $\delta^{18}O_{atm}$ values were < 1.0 ‰ during the pre-MPT glacial periods (Yan et al., 2019). The EPICA Dome C (EDC) record shows that Termination I, II, IV, V and VII are the only terminations that have both values of

310 negative and > 1.0 ‰ during the last 800 ka (Landais et al., 2013; Extier et al., 2018a) (Fig. 5). Hence, we exclude Termination III and VI for the Larsen BIA ages. Among the candidates, Termination V should also be excluded because the maximum $\delta^{18}O_{atm}$ value in the EDC record is ~1.4 ‰, which is significantly higher than that of the Larsen ice. The δ^2H_{ice} decrease in the middle of the glacial termination in the Larsen BIA (Fig. 4b) is similar to that during the Antarctic Cold Reversal (ACR, 14.6–

315 12.7 ka BP), which is a distinct feature only during Termination I among the candidate terminations (i.e., Termination I, II, IV and VII) as we see in the EDC δ^2H_{ice} record (Fig. 6). To confirm the age of the Larsen ice, we compared the $\delta^{18}O_{atm}$–CH_4 relationship with the ice from core #23 at depths of 4.6–10 m with the EDC and WAIS Divide (Fig. 7). We found that the Larsen $\delta^{18}O_{atm}$–CH_4 distribution was well matched only at Termination I. It appears that $\delta^{18}O_{atm}$ of Larsen has a 0.05 ‰ offset with that of the WAIS Divide. However, this offset is not odd, as we can also see a ~0.05 ‰ offset between core #23 and horizontal measurements at a depth of > 1.95 m; the offset may also come from age difference (Fig. A2). The $\delta^{18}O_{atm}$–CO_2 and

320 CO_2–CH_4 relationships do not clearly match with those of Termination I in the EDC and WAIS Divide records. The Larsen ice showed a higher CO_2 concentration of 10–20 ppm. Probably, it is altered naturally and/or contaminated, even at depths of 4.6–10 m (Fig. A3, Fig. A4). Finally, we confirmed the ages of the Larsen ice with ^{81}Kr dating, indicating 9–41 and 14–43 ka for ice from the TF and #23 cores, respectively (Table 1), and conclude that Larsen ice covers the Last Glacial Termination (LGT, T1).
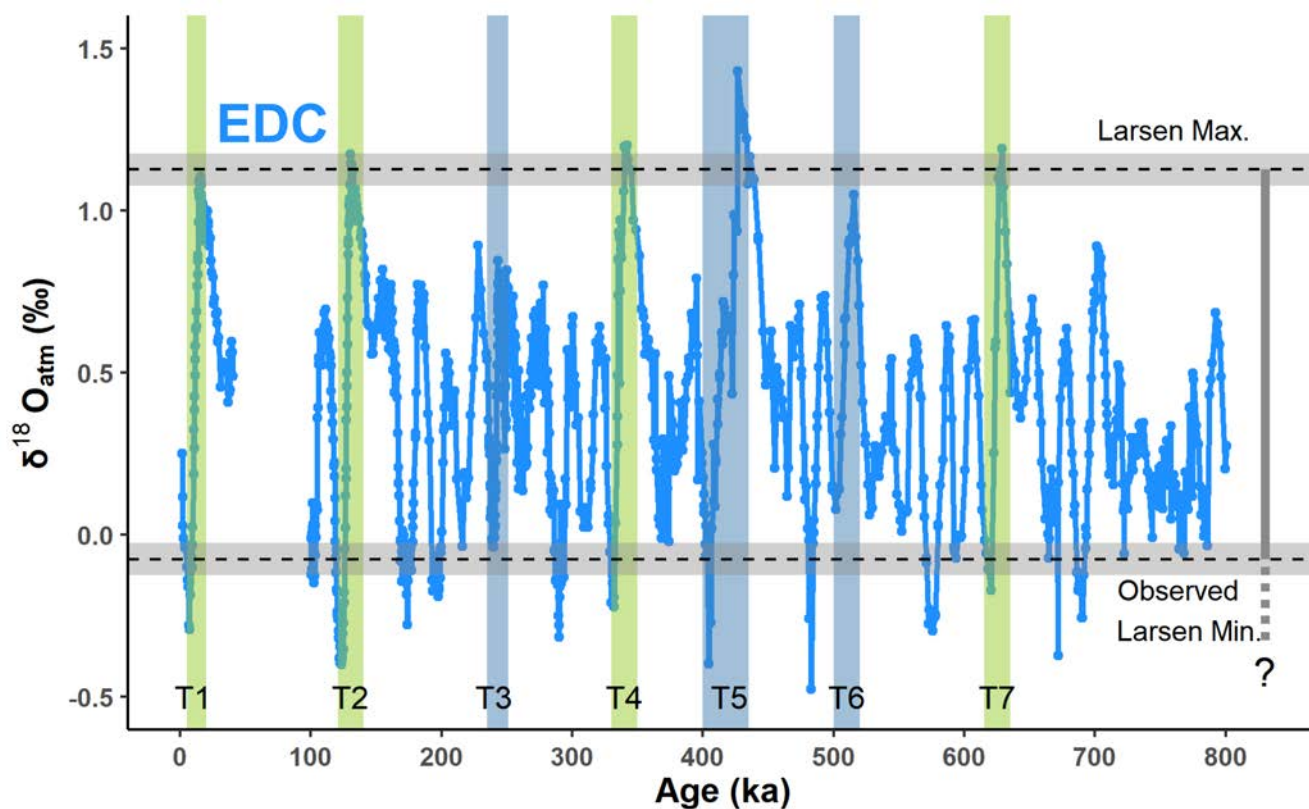
325

Figure 5. Comparison of Larsen $\delta^{18}O_{atm}$ with EDC record. $\delta^{18}O_{atm}$ records are from Landais et al. (2013) for 0–40 ka and Extier et al. (2018a) for 100–800 ka, respectively. Green vertical bars represent the candidate age intervals for Larsen blue ice; T, Termination. Observed Larsen $\delta^{18}O_{atm}$ value is shown as a vertical grey bar. Horizontal grey bars with dash lines represent the uncertainty of the measured $\delta^{18}O_{atm}$ from Larsen BIA (Fig. A2).

330
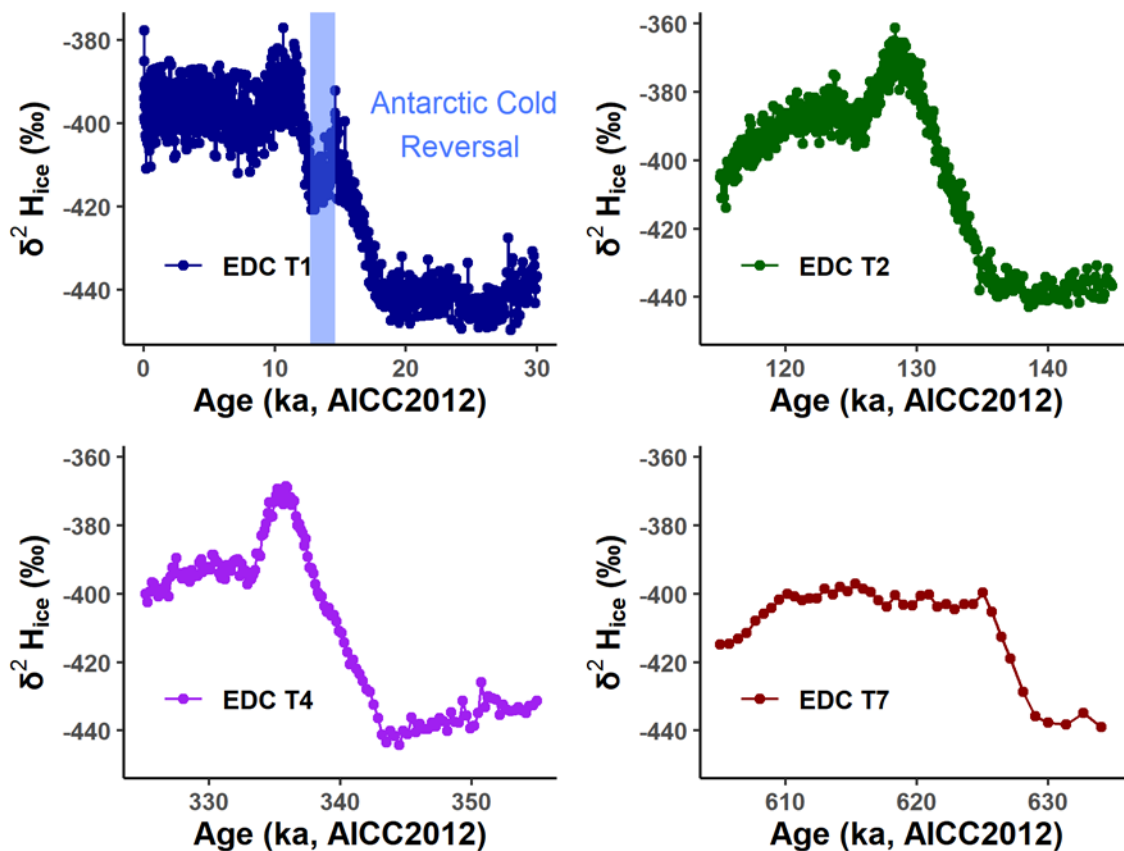
Figure 6. δ²H_ice records from EDC. $\delta^2 H_{ice}$ records for T1, T2, T4, and T7 on AICC2012 scale are from Bazin et al. (2013b). The blue vertical bar represents the time interval of the ACR (14.6–12.7 ka BP).
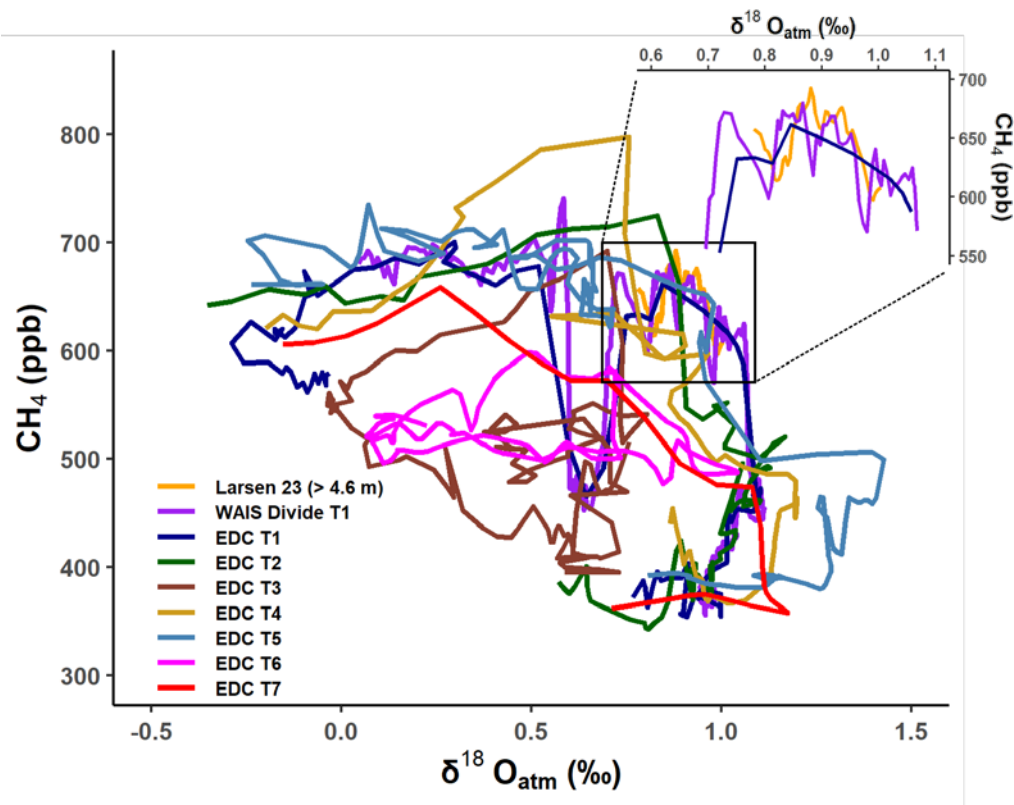
Figure 7. Comparison of $\delta^{18}O_{atm}$-CH_4 relationship in the Larsen ice core #23 with existing records during glacial Terminations.
$\delta^{18}O_{atm}$ and CH_4 data of WAIS Divide are from Severinghaus (2015) and Rhodes et al. (2017), respectively. $\delta^{18}O_{atm}$ of EDC is from Landais et al. (2013) and Extier et al. (2018a). CH_4 record of EDC is from Bazin et al. (2013d). The area within the black box is magnified to compare the Larsen #23 record with those from WAIS Divide T1 and EDC T1.

3.6 Gas and ice ages of Larsen ice

The CH_4 was severely altered at a depth of 1.95 m and the available CH_4 record was only from ice core #23 (> 4.6 m). Therefore, we developed the tentative gas age by correlating the horizontal $\delta^{18}O_{atm}$ value to the WAIS Divide record on the WD2014 timescale. Then, fine correlation was conducted with CH_4 record from the core #23, which corresponds to 13.3–14.1 ka at depths of 4.6–10.4 m (Fig. 8c). We take advantage of the high-resolution records of CH_4 from both Larsen core #23 and WAIS Divide ice, which greatly improves the precision of age construction. The following paragraph describes this process in detail.

Spline curves were created for both WAIS Divide and Larsen $\delta^{18}O_{atm}$ records to reduce artefact from insufficient sampling resolution and/or ice quality at a 1.95 m depth of the Larsen ice (Fig. 8). The spline curve was drawn after interpolating the original records at 5 m horizontal distance intervals. Three points were chosen, which divide the upstream part of the Larsen ice into three equal parts to tie with those in the WAIS Divide record (pink dots in Fig. 8a and 8b). For the downstream side of the Larsen ice, we chose a local maximum and a minimum as the tie points (purple dots in Fig. 8a and 8b) because the slope

350 of the $\delta^{18}O_{atm}$ spline curve is small. When the horizontal distance was greater than 1280 m, the age was constrained by extrapolation using the age/distance relationship at 18–22 ka. Based on the tentative horizontal gas ages and the depth/distance relationship of core #23 (obtained from Fig. 4b), we determined the gas age of core #23 (~10 m vertical ice core). A small offset (53.6 ± 38.5 yr) existed between the CH_4 record of core #23 (> 4.6 m) and the WAIS Divide record (offset between the red and dark blue lines in Fig. 8d). To eliminate this gap, four tie-points (orange dots) were chosen and interpolated (light blue

355 line). The gas age, corresponding to 13.3–14.1 ka was obtained more accurately by using the CH_4 correlation. As a result, the gas age for the Larsen ice at 1.95 m depth was estimated to be 9.2–23.4 ka BP on WAIS Divide chronology in 2014 (WD2014). The ages on AICC2012 scale were estimated to be 9.4–23.4 ka by using the depth and the WD2014 age of EDC (Bazin et al., 2013a, Buizert et al., 2021).
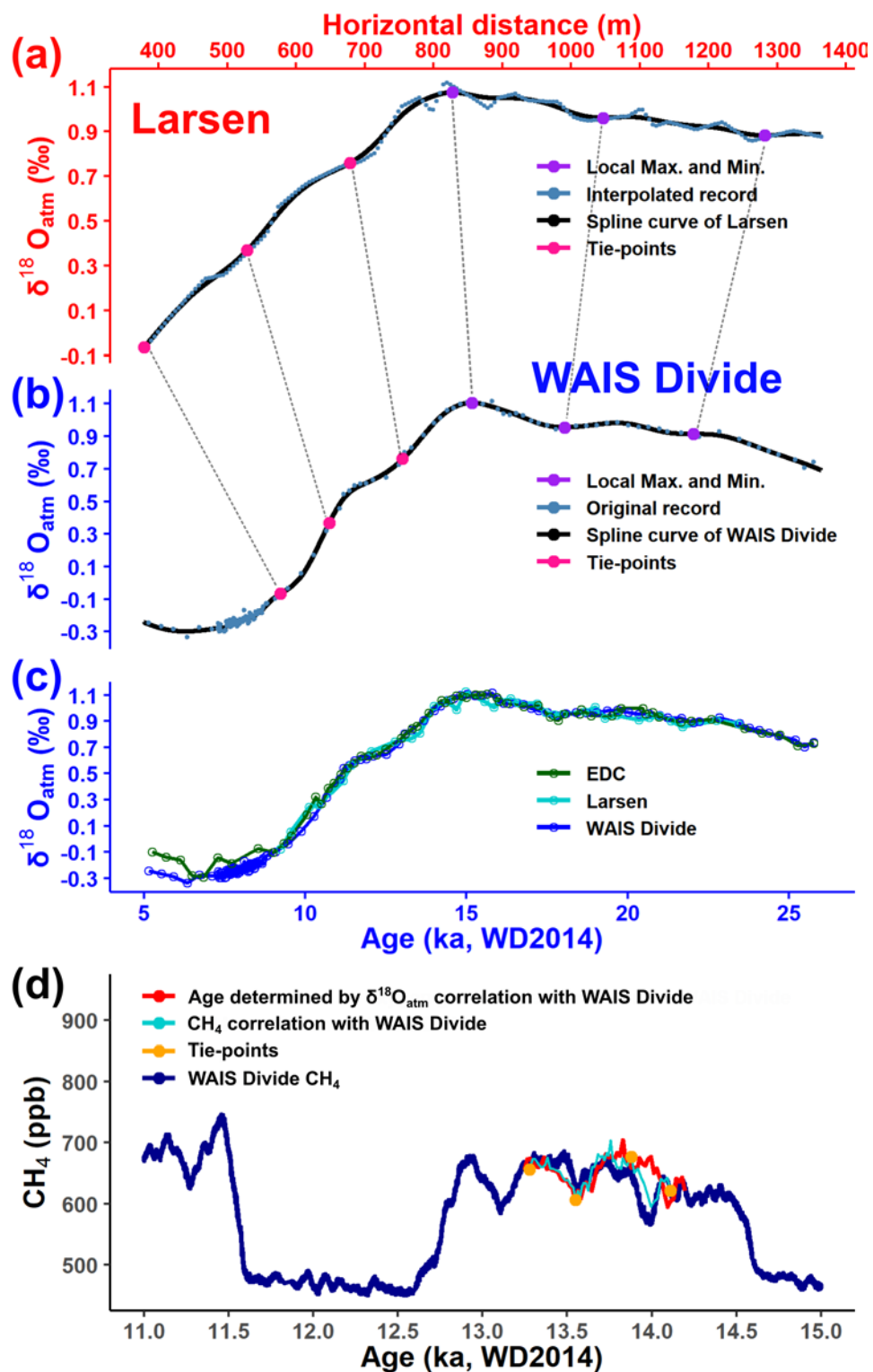
Figure 8. Correlation of Larsen δ^{18}O$_{atm}$ and CH$_4$ records with WAIS Divide. (a) 5 m interpolated δ^{18}O$_{atm}$ value from Larsen BIA with a spline curve. **(b)** δ^{18}O$_{atm}$ record from WAIS Divide with a spline curve (Severinghaus et al., 2015). Six tie-points were used to correlate each other. **(c)** Comparison of synchronized Larsen δ^{18}O$_{atm}$ with EDC (Landais et al., 2013) and WAIS Divide records. **(d)** Comparison of CH$_4$ record from Larsen #23 (> 4.6 m depth) with WAIS Divide (Rhodes et al., 2017). Tentative gas age determined by δ^{18}O$_{atm}$ correlation with WAIS Divide is tuned by correlating CH$_4$ record using four tie-points. WD2014 timescale for WAIS Divide and EDC is from Sigl et al. (2016) and Buizert et al. (2021), respectively.

The ice ages of the Larsen ice were determined based on the δ^{18}O$_{ice}$ correlation with the TALDICE record (Fig. 9). TALDICE was chosen because the coring site is close to the Larsen BIA (~240 km apart) and the direction of the TALDICE site from the Larsen BIA is similar to the ice flow direction of the Larsen ice (Rignot et al., 2011; Mouginot et al., 2012). It is likely that the trend of surface temperature changes in the snow accumulation zone of Larsen BIA is comparable to that of the TALDICE site. We constructed spline curves of the horizontal measurement of the surface ice. As described above, we interpolated the original δ^{18}O$_{ice}$ records at 5 m interval in order to avoid bias in the δ^{18}O$_{ice}$ record. The correlation was established by visually choosing a similar inflection point. Then, in order to validate the ice age, we estimated the ice age at 1.95 m depth (Appendix C for more information) and calculated the Δage; Δage for Larsen ice is defined as (ice age) − (gas age) at a depth of 1.95 m. It should be noted that the ice is older than the gas at the corresponding depth because the gas is isolated when the firn completely transforms into ice (Schwander and Stauffer, 1984).

First, eight tie-points were selected and linearly interpolated. In this case, Δage showed a minimum value at around 17.5 ka (Fig. A6), which is near to the time period of the Last Glacial Maximum (LGM). Since it is known that Δage increases when the climate is colder (Schwander et al., 1997), we assumed that either the ice age is undervalued or the gas age is overvalued. Because the δ^{18}O$_{atm}$ value of the Larsen ice is comparable with the EDC and WAIS Divide records, the gas age seems to be reasonable and not likely to be overvalued (Fig. 8). Hence, we concluded that the ice age should be revised. In addition, the age/distance relationship of ice shows a fast age increase near ~1000 m (Fig. A7), which is not supported by the average dip of the ice layer deduced from the GPR profile (Fig. 3). As the dip decreases to the downstream ice, an abrupt increase in the slope of the age/distance relationship is not expected. However, this is the case only when we assume no abrupt change in the snow accumulation rate.

After excluding one tie-point (indicated by the red dotted line in Fig. 9), the Δage of Larsen ice shows a maximum value at approximately 17.5 ka, which appears more appropriate (Fig. A6). For records with horizontal distances less than 107 m and greater than 1310 m, extrapolation was conducted to estimate the ice age using the age/distance relationship at 7–11 ka and 18–24 ka, respectively. In conclusion, the ice age was estimated to be 5.6–24.7 ka (WD2014) for the surface ice. However, as noted above, local age inversion might have occurred in the upstream ice areas. Hence, the age constraint for upstream ice should be considered cautiously. The ice age calculated for a 1.95 m depth also seems reliable because the water isotope record is comparable with the surface ice result when plotted with the ice age (Fig. 9c).
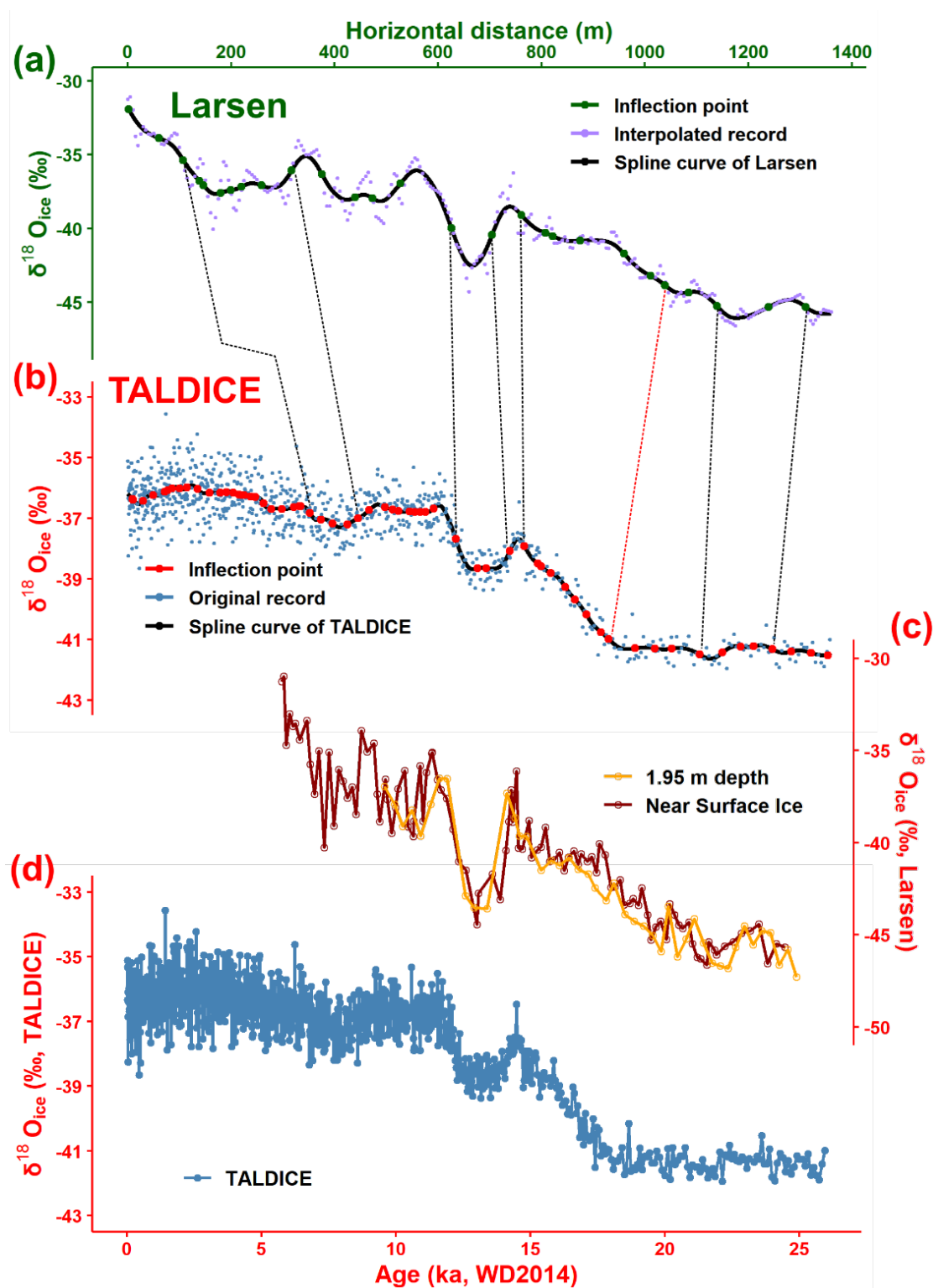
Figure 9. Correlation of Larsen $\delta^{18}O_{ice}$ with TALDICE record. (a) 5 m interpolated $\delta^{18}O_{ice}$ value from Larsen BIA with a spline curve.
(b) $\delta^{18}O_{ice}$ record from TALDICE with a spline curve (Stenni et al., 2010, Bazin et al., 2013c). The ice age of the surface ice from Larsen
395 was estimated by correlating 7 inflection points of the spline curve (indicated by black dotted lines) with TALDICE. **(c)** Comparison of near-
surface $\delta^{18}O_{ice}$ with those in 1.95 m depth at Larsen BIA. **(d)** $\delta^{18}O_{ice}$ record of TALDICE shown in more detail (Stenni et al., 2010, Bazin et
al., 2013c).

More precise ages may be obtained if additional ice is available for a higher sampling resolution. However, our data clearly

show that the studied Larsen ice ages cover the Last Glacial Maximum, Last Glacial Termination, and early Holocene, and we

400 may obtain reliable records for surface temperature at the original snow accumulation sites and atmospheric greenhouse gas

concentrations, although the latter is not guaranteed for depths < 4–10 m, depending on the gas species. Assuming that the

average age/depth relationship of ice core #23 (~156 yr m^{-1}) is maintained throughout the ice, the age may reach ~50 ka near

the bedrock (~240 m of ice). Thus, ice may be obtained at least ~50 ka by shallow coring at the Larsen BIA.

4 Conclusions

405 Based on the dust bands, GPR profile, and no significant anomaly of chemical results ($\delta^{18}O_{atm}$, δ^2H_{ice}, and CH_4) we conclude

that the ages of the downstream ice in Larsen BIA monotonically increase along the ice flow direction. The correlation of

δ^2H_{ice} values, which are from ice core #23 and the surface ice samples, also shows that the stratigraphy of ice is not significantly

disturbed and does not cause an age inversion at the site. CH_4 is well-preserved in ice core #23 at a depth of > 4.6 m, and gas

isotopes ($\delta^{18}O_{atm}$, $\delta^{15}N$-N_2) are well-preserved at 1.95 m depth. Horizontal $\delta^{18}O_{atm}$ values at a depth of 1.95 m in the Larsen

410 BIA reveal a very typical glacial termination. Along with the stable water isotopes, correlation of CH_4 concentration, and

$\delta^{18}O_{atm}$ with existing ice core records, the gas ages of the studied Larsen ice cover 9.2–23.4 ka. In addition, the ^{81}Kr ages from

#23 and TF cores also support the age. We provide high-precision ages for ice and fossil air trapped in blue ice at the Larsen

Glacier. Because well-constrained ages and high quality of proxies are essential for paleoclimate study, our work may help

future studies for blue ice in the Northern Victoria Land. Especially, since large amount of ice with the same age is exposed at

415 the surface in the BIA, this study may lead to further research on paleoclimate that was difficult because of the limited amount

of ice samples.

Appendix A: CH$_4$, CO$_2$, δ^{18}O$_{atm}$, and δ^{15}N-N$_2$ measurements of the Larsen Glacier
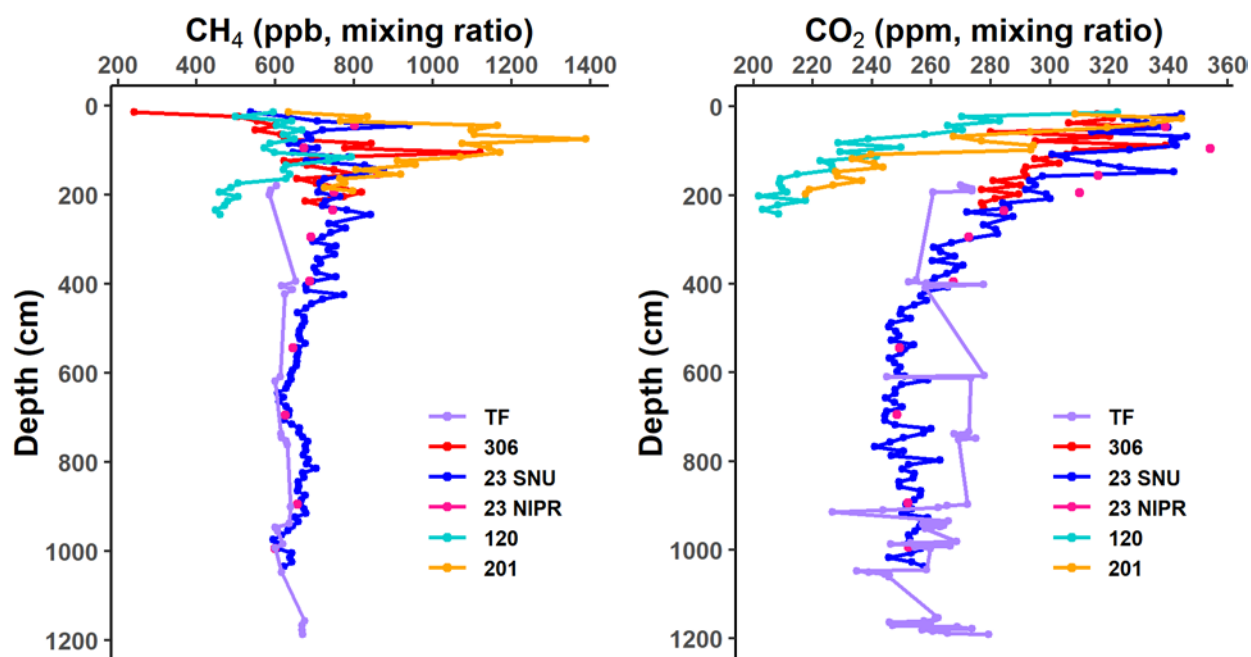
Figure A1. Vertical profiles of greenhouse gas concentrations at Larsen BIA ice cores. (a) CH$_4$ records. **(b)** CO$_2$ records. CH$_4$ was
420 measured by wet extraction, while CO$_2$ by both dry and wet extraction methods at SNU and NIPR, respectively. Results of TF core are from
Jang et al. (2017).
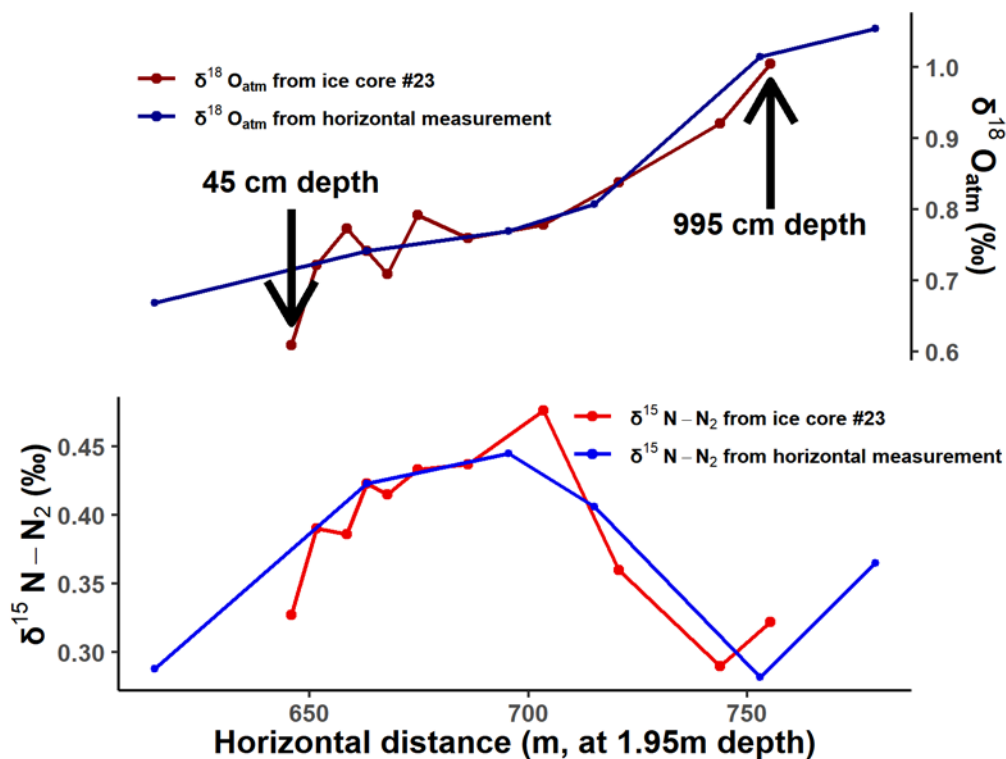
Figure A2. Nitrogen and oxygen gas isotope record of ice core #23 and horizontal measurement. Horizontal measurement is conducted using ice cores at 1.95 m depth. Depth of ice core #23 was converted to horizontal distance at 1.95 m depth by using Eq. (3). The uncertainty of measured $\delta^{18}O_{atm}$ at a depth of 1.95 m is assumed to be ± 0.05 ‰, which was deduced by the offset between the dark-red and dark-blue line.

430

435

440

Appendix B: Gas age estimation for the Larsen Glacier
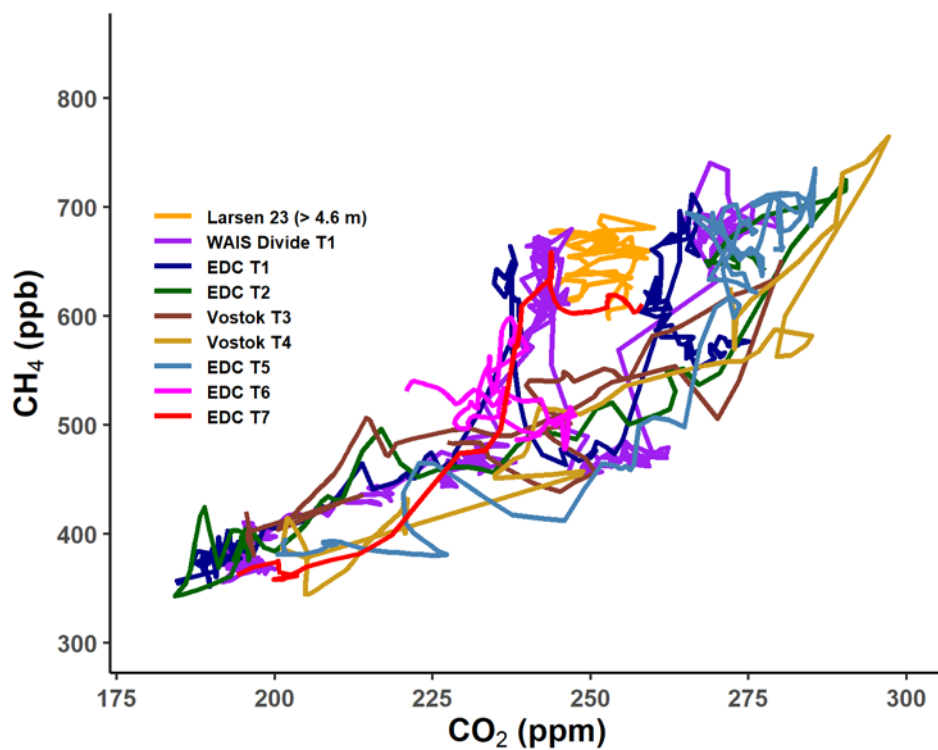
Figure A3. Comparison of CO₂−CH₄ relationship in the Larsen ice core #23 with existing records during glacial Terminations. WAIS
Divide: Marcott et al. (2014); Rhodes et al. (2017); EDC: Bazin et al. (2013d); Monnin et al. (2001); Monnin et al. (2004); Siegenthaler et
445 al. (2005); Lourantou et al. (2010); Schmitt et al. (2012); Bereiter et al. (2015); Vostok: Petit et al. (1999).
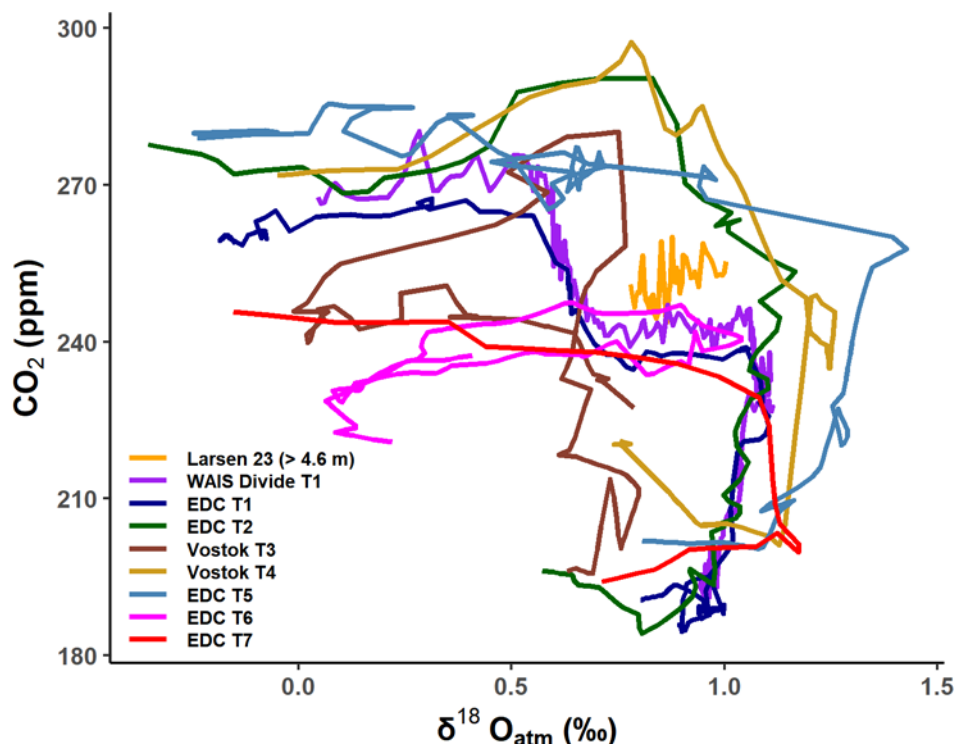
Figure A4. Comparison of δ¹⁸O$_{atm}$–CO₂ relationship in the Larsen ice core #23 with existing records during glacial Terminations.
WAIS Divide: Marcott et al. (2014); Severinghaus et al. (2015); EDC: Monnin et al. (2001); Monnin et al. (2004); Siegenthaler et al. (2005); Lourantou et al. (2010); Schmitt et al. (2012); Landais et al. (2013); Bereiter et al. (2015); Extier et al. (2018a); Vostok: Petit et al. (1999); Bender (2002).

Appendix C: Ice age estimation for the Larsen Glacier

To estimate the ice age at a depth of 1.95 m, the age/depth relationship of each ice core sample must be known. The relation is deduced by a simple calculation using Eq. (A1) and (A2); α, β, γ: ice age at each location; D: horizontal distance between two surface ice samples (at a depth of 20 cm); θ is the average dip of the ice layer; H + 0.2 m: depth where the age is the same as β. The average dip was estimated from the GPR profile (yellow box in Fig. 3c). The average dip of the ice layer located near core #23 was 4.96°, as inferred from Fig. 4b. Then, the ice age at a depth of 1.95 m was calculated using Eq. (A3). Refer to Fig. A5 to understand the following equations:

$$H = D \times \tan\theta \tag{A1}$$

$$\text{Age/depth relation} = (\beta-\alpha)/H \tag{A2}$$

$$\gamma = \{(\beta-\alpha)/H\} \times (1.95-0.2) + \alpha \tag{A3}$$
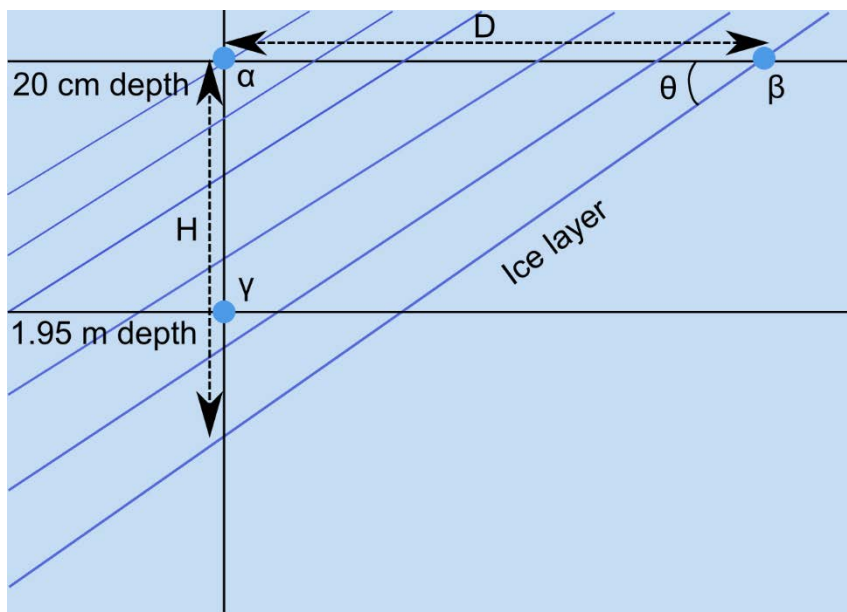
Figure A5. Schematic illustration for mathematical relation between ice ages.
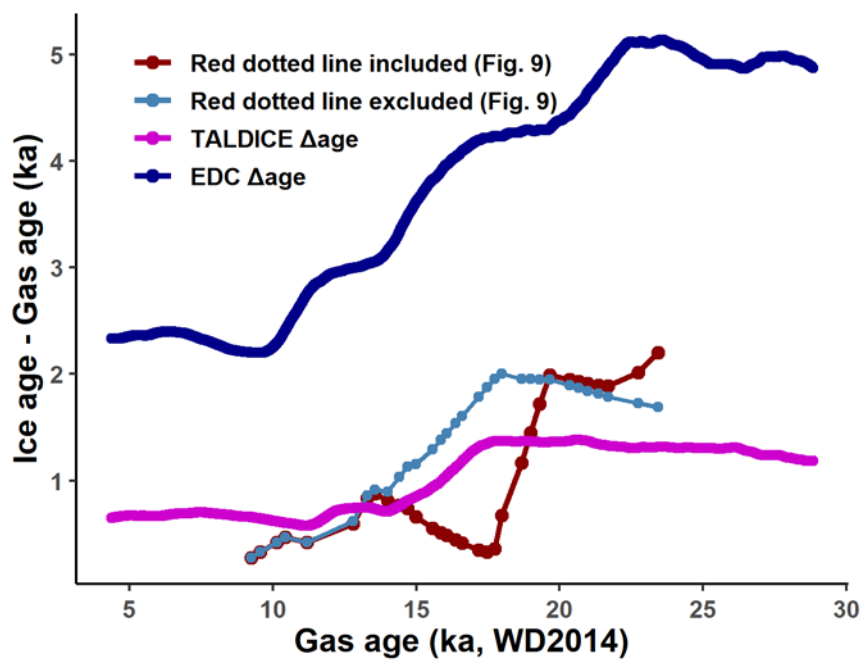
465   **Figure A6. EDC, TALDICE and Larsen BIA Δage.** Δage for Larsen BIA is defined as (ice age) − (gas age) at 1.95 m depth. EDC WD2014 chronology is from Buizert et al. (2021).
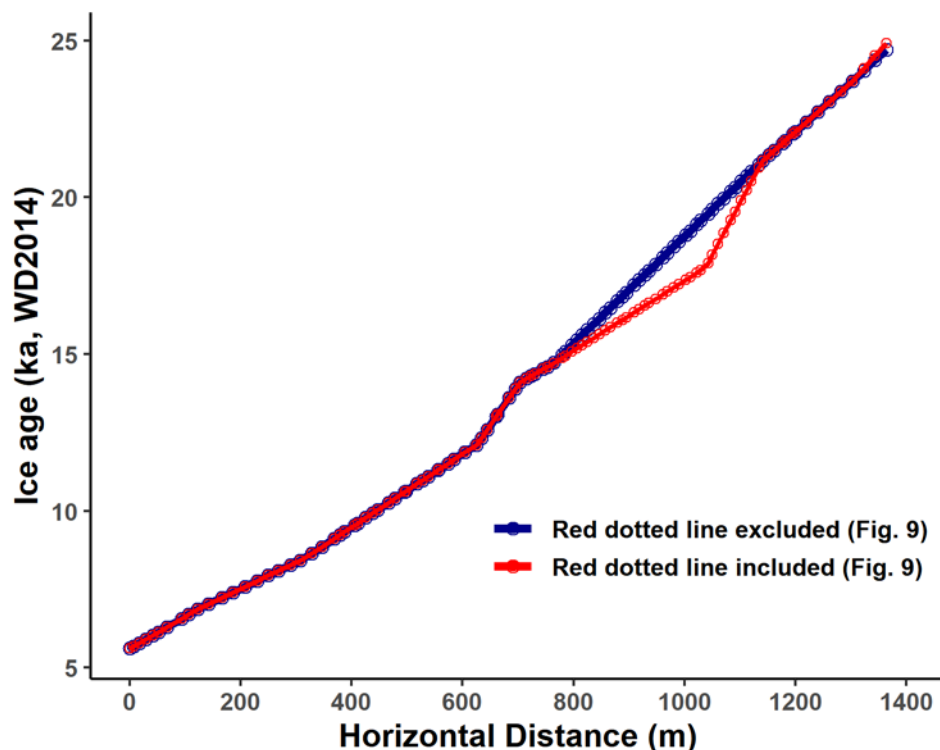
Figure A7. Relation between horizontal distance and ice age.

Author contributions

470   GL and JA conceived the idea of this study, performed experiments, interpreted the data, and wrote the manuscript with contributions from all the co-authors. HJ performed the ground penetrating radar surveys and data processing. FR, Z.-TL, WJ, and GY carried out [81]Kr age dating of Larsen Glacier. IO, SG, and KK assisted the gas measurements at NIPR and interpretation of the results. SK and JM measured the stable water isotopes of the ice. CB established the WD2014 timescale of the TALDICE. SH, CHH, SDH helped collect the ice samples and organizing the early plans of this study. All authors discussed and interpreted

475   the results and contributed to the manuscript.

Competing interests

    The authors declare that they have no conflict of interest.

Acknowledgements

We thank Sang-Young Han, Yoojung Yang, Youngjoon Jang, and Yeongcheol Han for their assistance in collecting ice and
480   organizing data in the early stage of the study. We sincerely thank Gwangjin Lim, Junghwa Hwang, and Jaeyoung Park for
their laboratory assistance and technical support. We thank Joohan Lee for providing the GPR survey equipment. We also
thank the Norwegian Polar Institute for sharing the QGIS Quantarctica package. We also appreciate the Meteo-Climatological
Observatory at MZS and Victoria Land of PNRA for annual surface temperature data at the Larsen Glacier.

Financial support

485   This study has been supported by the Korea Polar Research Institute (grant no. PE21100) and National Research Foundation
of Korea (NRF-2018R1A2B3003256). This work has also received financial support from the National Key Research and
Development Program of China (2016YFA0302200), National Natural Science Foundation of China (41727901), the Japan
Society for the Promotion of Science (JSPS) and the Ministry of Education, Culture, Sports, Science and Technology of Japan
(MEXT) KAKENHI grant numbers 17K12816 to IO; 17H06320 and 15KK0027 to KK, and NIPR International Internship
490   Program for Polar Science to GL.

References

Aarons, S. M., Aciego, S. M., Arendt, C. A., Blakowski, M. A., Steigmeyer, A., Gabrielli, P., Sierra-Hernández, M. R.,
Beaudon, E., Delmonte, B., Baccolo, G., May, N. W., and Pratt, K. A.: Dust composition changes from Taylor Glacier
(East Antarctica) during the last glacial-interglacial transition: A multi-proxy approach, Quaternary Sci. Rev., 162, 60–71,
495   https://doi.org/10.1016/j.quascirev.2017.03.011, 2017.

Aciego, S. M., Cuffey, K. M., Kavanaugh, J. L., Morse, D. L., and Severinghaus, J. P.: Pleistocene ice and paleo-strain rates
at Taylor Glacier, Antarctica, Quaternary Res., 68, 303–313, https://doi.org/10.1016/j.yqres.2007.07.013, 2007.

Ahn, J., Brook, E. J., and Howell, K.: A high-precision method for measurement of paleoatmospheric CO_2 in small polar ice
samples, J. Glaciol., 55, 499–506, https://doi.org/10.3189/002214309788816731, 2009.

500   Azuma, N., Nakawo, A., Higashi, A., and Nishio, F.: Flow pattern near Massif A in the Yamato bare ice field estimated from
the structures and the mechanical properites of a shallow ice core, Memoirs of National Institute of Polar Research. Special
issue, 39, 173–183, 1985.

Baggenstos, D., Bauska, T. K., Severinghaus, J. P., Lee, J. E., Schaefer, H., Buizert, C., Brook, E. J., Shackleton, S., and
Petrenko, V. V.: Atmospheric gas records from Taylor Glacier, Antarctica, reveal ancient ice with ages spanning the entire
505   last glacial cycle, Clim. Past, 13, 943–958, https://doi.org/10.5194/cp-13-943-2017, 2017.

Baggenstos, D., Severinghaus, J. P., Mulvaney, R., McConnell, J. R., Sigl, M., Maselli, O., Petit, J.R., Grente, B., and Steig, E. J.: A horizontal ice core from Taylor Glacier, its implication for Antarctic climate history, and an improved Taylor Dome ice core time scale, Paleoceanography and Paleoclimatology, 33, 778−794, https://doi.org/10.1029/2017PA003297, 2018.

Bauska, T., Baggenstos, D., Brook, E. J., Mix, A. C., Marcott, S. A., Petrenko, V. V., Schaefer, H., Severinghaus, J. P., and Lee, J. E.: Carbon isotopes characterize rapid changes in atmospheric carbon dioxide during the last deglaciation, P. Natl. Acad. Sci. USA, 113, 3465–3470, https://doi.org/10.1073/pnas.1513868113, 2016.

Bazin, L., Landais, A., Lemieux-Dudon, B., Toyé Mahamadou Kele, H., Veres, D., Parrenin, F., Martinerie, P., Ritz, C., Capron, E., Lipenkov, V. Y., Loutre, M.-F., Raynaud, D., Vinther, B. M., Svensson, A. M., Rasmussen, S. O., Severi, M., Blunier, T., Leuenberger, M. C., Fischer, H., Masson-Delmotte, V., Chappellaz, J. A., and Wolff, E. W.: AICC2012 chronology for ice core EDC, PANGAEA, https://doi.org/10.1594/PANGAEA.824865, 2013a.

Bazin, L., Landais, A., Lemieux-Dudon, B., Toyé Mahamadou Kele, H., Veres, D., Parrenin, F., Martinerie, P., Ritz, C., Capron, E., Lipenkov, V. Y., Loutre, M.-F., Raynaud, D., Vinther, B. M., Svensson, A. M., Rasmussen, S. O., Severi, M., Blunier, T., Leuenberger, M. C., Fischer, H., Masson-Delmotte, V., Chappellaz, J. A., and Wolff, E. W.: delta Deuterium measured on ice core EDC on AICC2012 chronology, PANGAEA, https://doi.org/10.1594/PANGAEA.824891, 2013b.

Bazin, L., Landais, A., Lemieux-Dudon, B., Toyé Mahamadou Kele, H., Veres, D., Parrenin, F., Martinerie, P., Ritz, C., Capron, E., Lipenkov, V. Y., Loutre, M.-F., Raynaud, D., Vinther, B. M., Svensson, A. M., Rasmussen, S. O., Severi, M., Blunier, T., Leuenberger, M. C., Fischer, H., Masson-Delmotte, V., Chappellaz, J. A., and Wolff, E. W.: delta ^{18}O measured on ice core TALDICE on AICC2012 chronology, PANGAEA, https://doi.org/10.1594/PANGAEA.824890, 2013c.

Bazin, L., Landais, A., Lemieux-Dudon, B., Toyé Mahamadou Kele, H., Veres, D., Parrenin, F., Martinerie, P., Ritz, C., Capron, E., Lipenkov, V. Y., Loutre, M.-F., Raynaud, D., Vinther, B. M., Svensson, A. M., Rasmussen, S. O., Severi, M., Blunier, T., Leuenberger, M. C., Fischer, H., Masson-Delmotte, V., Chappellaz, J. A., and Wolff, E. W.: Methane measured on ice core EDC on AICC2012 chronology, PANGAEA, https://doi.org/10.1594/PANGAEA.824883, 2013d.

Bender, M., Labeyrie, L. D., Raynaud, D., and Lorius, C.: Isotopic composition of atmospheric O_2 in ice linked with deglaciation and global primary productivity, Nature, 318, 349–352, https://doi.org/10.1038/318349a0, 1985.

Bender, M.: Concentration and Isotopic Composition of O2 and N2 in Trapped Gases of the Vostok Ice Core, U.S. Antarctic Program (USAP) Data Center, https://doi.org/10.7265/N5862DCW, 2002.

Bereiter, B., Eggleston, S., Schmitt, J., Nehrbass-Ahles, C., Stocker, T. F., Fischer, H., Kipfstuhl, S., and Chappellaz, J.: Revision of the EPICA Dome C CO_2 record from 800 to 600 kyr before present, Geophys. Res. Lett., 42, 542−549, doi:10.1002/2014GL061957, 2015.

Bindschadler, R., Vornberger, P., Fleming, A., Fox, A., Mullins, J., Binnie, D., Paulsen, S. J., Granneman, B., and Gorodetzky, D.: The Landsat image mosaic of Antarctica, Remote Sens. Environ., 112, 4214–4226, https://doi.org/10.1016/j.rse.2008.07.006, 2008.

Bintanja, R.: On the glaciological, meteorological, and climatological significance of Antarctic blue ice areas, Rev. Geophys., 37, 337–359, https://doi.org/10.1029/1999RG900007, 1999.

540 Blunier, T. and Brook, E. J.: Timing of millennial-scale climate change in Antarctica and Greenland during the last glacial period, Science, 291, 109−112, https://doi.org/10.1126/science.291.5501.109, 2001.

Blunier, T., Spahni, R., Barnola, J.-M., Chappellaz, J., Loulergue, L., and Schwander, J.: Synchronization of ice core records via atmospheric gases, Clim. Past, 3, 325–330, https://doi.org/10.5194/cp-3-325-2007, 2007.

Borgorodsky, V. V., Bentley, C. R., Gudmandsen, P. E.: Radioglaciology, 1, Glaciology and Quaternary Geology, Springer

545 Netherlands, doi: 10.1007/978-94-009-5275-1, 1985.

Buizert, C., Baggenstos, D., Jiang, W., Purtschert, R., Petrenko, V. V., Lu, Z.-T., Müller, P., Kuhl, T., Lee, J., Severinghaus, J. P., and Brook, E. J.: Radiometric ^{81}Kr dating identifies 120,000-year-old ice at Taylor Glacier, Antarctica, P. Natl. Acad. Sci. USA., 111, 6876–6881, https://doi.org/10.1073/pnas.1320329111, 2014.

Buizert, C., Cuffey, K. M., Severinghaus, J. P., Baggenstos, D., Fudge, T. J., Steig, E. J., Markle, B. R., Winstrup, M., Rhodes,

550 R. H., Brook, E. J., Sowers, T. A., Clow, G. D., Cheng, H., Edwards, R. L., Sigl, M., McConnell, J. R., and Taylor, K. C.: The WAIS Divide deep ice core WD2014 chronology – Part 1: Methane synchronization (68–31 ka BP) and the gas age– ice age difference, Clim. Past, 11, 153–173, https://doi.org/10.5194/cp-11-153-2015, 2015.

Buizert, C., Sigl, M., Severi, M., Markle, B. R., Wettstein, J. J., McConnell, J. R., Pedro, J. B., Sodemann, H., Goto-Azuma, K., Kawamura, K., Fuita, S., Motoyama, H., Hirabayashi, M., Uemura, R., Stenni, B., Parrenin, F., He, F., Fudge, T. J.,

555 and Steig, E. J.: Abrupt ice-age shifts in southern westerly winds and Antarctic climate forced from the north, Nature, 563, 681–685, https://doi.org/10.1038/s41586-018-0727-5, 2018.

Buizert, C., Fudge, T. J., Roberts, W. H. G., Steig, E. J., Sherriff-Tadano, S., Ritz, C., Lefebvre, E., Edwards, J., Kawamura, K., Oyabu, I., Motoyama, H., Kahle, E. C., Jones, T. R., Abe-Ouchi, A., Obase, T., Martin, C., Corr, H., Severinghaus, J. P., Beaudette, R., Epifanio, J. A., Brook, E. J., Martin, K., Chappellaz, J., Aoki, S., Nakazawa, T., Sower, T. A., Alley, R.

560 B., Ahn, J., Sigl, M., Severi, M., Dunbar, N. W., Svensson, A., Fegyveresi, J. M., He, C., Liu, Z., Zhu, J., Otto-Bliesner, B. L., Lipenkov, V. Y., Kageyama, M., and Schwander, J.: Antarctic surface temperature and elevation during the Last Glacial Maximum, Science, 372, 1097–1101, DOI: 10.1126/science.abd2897, 2021.

Capron, E., Landais, A., Leieux-Dudon, B., Schilt, A., Masson-Delmotte, V., Buiron, D., Chappellaz, J., Dahl-Jensen, D., Johnsen, S., Leuenberger, M., Loulergue, L., and Oerter, H.: Synchronising EDML and NorthGRIP ice cores using δ^{18}O

565 of atmospheric oxygen (δ^{18}O$_{atm}$) and CH$_4$ measurements over MIS5 (80−123 kyr), Quaternary Sci. Rev., 29, 222−234, https://doi.org/10.1016/j.quascirev.2009.07.014, 2010.

Cassidy, W., Harvey, R., Schutt, J., Delisle, G., and Yanai, K.: The meteorite collection sites of Antarctica, Meteoritics, 27, 490–525, https://doi.org/10.1111/j.1945-5100.1992.tb01073.x, 1992.

Chalk, T. B., Hain, M. P., Foster, G. L., Rohling, E. J., Sexton, P. F., Badger, M. P. S., Cherry, S. G., Hasenfratz, A. P., Haug,

570 G. H., Jaccard, S. L., Martínez-García, A., Pälike, H., Pancost, R. D., and Wilson, P. A.: Causes of ice age intensification

across the Mid-Pleistocene Transition, P. Natl. Acad. Sci. USA., 114, 13114–13119, https://doi.org/10.1073/pnas.1702143114, 2017.

Craig, H., Horibe, Y., and Sowers, T.: Gravitational Separation of Gases and Isotopes in Polar Ice Caps, Science, 242, 1675–1678, doi: 10.1126/science.242.4886.1675, 1988.

575 Crotti, I., Landais, A., Stenni, B., Bazin, L, Parrenin, F., Frezzotti, M., Ritterbusch, F., Lu, Z.-T., Jiang, W., Yang, G.-M., Fourré, E., Orsi, A., Jacob, R., Minster, B., Prié, F., Dreossi, G., and Barbante, C.: An extension of the TALDICE ice core age scale reaching back to MIS 10.1, Quaternary Sci. Rev., 266, 107078, https://doi.org/10.1016/j.quascirev.2021.107078, 2021.

Curzio, P., Folco, L., Laurenzi, M. A., Mellini, M., and Zeoli, A.: A tephra chronostratigraphic framework for the Frontier
580 Mountain blue-ice field (northern Victoria Land, Antarctica), Quaternary Sci. Rev., 27, 602–620, https://doi.org/10.1016/j.quascirev.2007.11.017, 2008.

Dansgaard, W., White, J., and Johnsen, S.: The abrupt termination of the Younger Dryas climate event, Nature, 339, 532–534, https://doi.org/10.1038/339532a0, 1989.

Delmas, R. J., Ascencio, J.-M, and Legrand, M.: Polar ice evidence that atmospheric CO_2 20,000yr BP was 50% of present,
585 Nature, 284, 155–157, https://doi.org/10.1038/284155a0, 1980.

Dlugokencky, E. J., Myers, R. C., Lang, P. M., Masarie, K. A., Crotwell, A. M., Thoning, K. W., Hall, B. D., Elkins, J. W., and Steele, L. P.: Conversion of NOAA atmospheric dry air CH_4 mole fractions to a gravimetrically prepared standard scale, J. Geophys. Res., 110, D18306, https://doi.org/10.1029/2005JD006035, 2005.

Dunbar, N. W., McIntosh, W. C., and Esser, R. P.: Physical setting and tephrochronology of the summit caldera ice record at
590 Mount Moulton, West Antarctica, Geol. Soc. Am. Bull., 120, 796−812, https://doi.org/10.1130/B26140.1, 2008.

Elderfield, H., Ferretti, P., Greaves, M., Crowhurst, S., McCave, I. N., Hodell, D., and Piotrowski, A. M.: Evolution of Ocean Temperature and Ice Volume Through the Mid-Pleistocene Climate Transition, Science, 337, 704−709, doi: 10.1126/science.1221294, 2012.

EPICA Community Members (2004).: Eight glacial cycles from an Antarctic ice core, Nature, 429, 623−628,
595 https://doi.org/10.1038/nature02599, 2004.

Extier, T., Landais, A., Bréant, C., Prié, F., Bazin, L., Dreyfus, G., Roche, D. M., and Leuenberger, M.: $\delta^{18}O_{atm}$ records between 100–800 ka from EPICA Dome C ice core, PANGAEA, https://doi.org/10.1594/PANGAEA.887323, 2018a.

Extier, T., Landais, A., Bréant, C., Prié, F., Bazin, L., Dreyfus, G., Roche, D. M., and Leuenberger, M.: On the use of $\delta^{18}O_{atm}$ for ice core dating, Quaternary Sci. Rev., 185, 244–257, https://doi.org/10.1016/j.quascirev.2018.02.008, 2018b.

600 Fischer, H., Severinghaus, J., Brook, E., Wolff, E., Albert, M., Alemany, O., Arthern, R., Bentley, C., Blankenship, D., Chappellaz, J., Creyts, T., Dahl-Jensen, D., Dinn, M., Frezzotti, M., Fujita, S., Gallee, H., Hindmarsh, R., Hudspeth, D., Jugie, G., Kawamura, K., Lipenkov, V., Miller, H., Mulvaney, R., Parrenin, F., Pattyn, F., Ritz, C., Schwander, J., Steinhage,

D., van Ommen, T., and Wilhelms, F.: Where to find 1.5 million yr old ice for the IPICS ″Oldest-Ice″ ice core, Clim. Past, 9, 2489–2505, https://doi.org/10.5194/cp-9-2489-2013, 2013.

605 Fogwill, C. J., Turney, C. S. M., Menviel, L., Baker, A., Weber, M. E., Ellis, B., Thomas, Z. A., Golledge, N. R., Etheridge, D., Rubino, M., Thornton., D. P., Van Ommen, T. D., Moy, A. D., Curran, M. A. J., Davies, S., Bird, M. I., Munksgaard, N. C., Rootes, C. M., Millman, H., Vohra, J., Rivera, A., Mackintosh, A., Pike, J., Hall, I. R., Bagshaw, E. A., Rainsley, E., Bronk-Ramsey, C., Montenari, M., Cage, A. G., Harris, M. R. P., Jones, R., Power, A., Love, J., Young, J., Weyrich, L. S., and Cooper, A.: Southern Ocean carbon sink enhanced by sea-ice feedbacks at the Antarctic Cold Reversal, Nat.
610 Geosci., 13, 489–497, https://doi.org/10.1038/s41561-020-0587-0, 2020.

Folco, L., Welten, K. C., Jull, A. J. T., Nishiizumi, K., and Zeoli, A.: Meteorites constrain the age of Antarctic ice at the Frontier Mountain blue ice field (northern Victoria Land), Earth Planet Sc. Lett., 248, 209–216, https://doi.org/10.1016/j.epsl.2006.05.022, 2006.

Goujon, C., Barnola, J.-M., and Ritz, C.: Modeling the densification of polar firn including heat diffusion: Application to close-
615 off characteristics and gas isotopic fractionation for Antarctica and Greenland sites, J. Geophys. Res., 108, 4792, https://doi.org/10.1029/2002JD003319, 2003.

Hall, B. D., Crotwell, A. M., Kitzis, D. R., Mefford, T., Miller, B. R., Schibig, M. F., and Tans, P. P.: Revision of the World Meteorological Organization Global Atmosphere Watch (WMO/GAW) CO2 calibration scale, Atmos. Meas. Tech., 14, 3015–3032, https://doi.org/10.5194/amt-14-3015-2021, 2021.

620 Harvey, R.: The Origin and Significance of Antarctic Meteorites, Geochemistry, 63, 93–147, https://doi.org/10.1078/0009-2819-00031, 2003.

Herron, M. M., and Langway, C. C.: Firn densification: An empirical model, J. Glaciol., 25, 373–385, doi:10.3189/S0022143000015239, 1980.

Higgins, J. A., Kurbatov, A. V., Spaulding, N. E., Brook, E., Introne, D. S., Chimiak, L. M., Yan, Y., Mayewski, P. A., and
625 Bender, M. L.: Atmospheric composition 1 million years ago from blue ice in the Allan Hills, Antarctica, P. Natl. Acad. Sci. USA., 112, 6887–6891, https://doi.org/10.1073/pnas.1420232112, 2015.

Hui, F., Ci, T., Cheng, X., Scambo, T. A., Liu, Y., Zhang, Y., Chi, Z., Huang H., Wang, X., Wang, F., Zhao, C., Jin, Z., and Wang, K.: Mapping blue-ice areas in Antarctica using ETM+ and MODIS data, Ann. Glaciol., 55, 129–137, doi:10.3189/2014AoG66A069, 2014.

630 Ikeda-Fukazawa, T., Fukumizu, K., Kawamura, K., Aoki, S., Nakazawa, T., and Hondoh, T.: Effects of molecular diffusion on trapped gas composition in polar ice cores, Earth Planet. Sc. Lett., 299, 183–192, https://doi.org/10.1016/j.epsl.2004.11.011, 2005.

Jang, Y., Han, Y., Ryu, Y., Moon, J., Ju, H.-T., Yang, J.-W., Lee, H.-G., Jun, S. J., Lee, J., Hur, S. D., Lee, J. I., and Ahn, J.: A preliminary study for blue ice in Victoria Land, East Antarctica, Journal of the Geological Society of Korea, 53, 567–
635 580, http://dx.doi.org/10.14770/jgsk.2017.53.4.567, 2017.

Jiang, W., Bailey, K., Lu, Z.-T., Mueller, P., O'Connor, T. P., Cheng, C.-F., Hu, S.-M., Purtschert, R., Sturchio, N. C., Sun, Y. R., Williams, W. D., and Yang, G.-M.: An atom counter for measuring ^{81}Kr and ^{85}Kr in environmental samples, Geochim. Cosmochim. Ac., 91, 1–6, https://doi.org/10.1016/j.gca.2012.05.019, 2012.

Jiang, W., Hu, S.-M., Lu, Z.-T., Ritterbusch, F., Yang, G.: Latest development of radiokrypton dating – A tool to find and study paleogroundwater, Quatern. Int., 547, 166–171, https://doi.org/10.1016/j.quaint.2019.04.025, 2020.

Jouzel, J., Alley, R. B., Cuffey, K. M., Dansgaard, W., Grootes, P., Hoffmann, G., Johnsen, S. J., Koster, R. D., Peel, D., Shuman, C. A., Stievenard, M., Stuiver, M., and White, J.: Validity of the temperature reconstruction from water isotopes in ice cores, J. Geophys. Res., 102, 26471–26487, https://doi.org/10.1029/97JC01283, 1997.

Korotkikh, E. V., Mayewski, P. A., Handley, M. J., Sneed, S. B., Introne, D. S., Kurbatov, A. V., Dunbar, N. W., and McIntosh, W. C.: The last interglacial as represented in the glaciochemical record from Mount Moulton Blue Ice Area, West Antarctica, Quaternary Sci. Rev., 30, 1940–1947, https://doi.org/10.1016/j.quascirev.2011.04.020, 2011.

Landais, A., Caillon, N., Severinghaus, J., Jouzel, J., and Masson-Delmotte, V.: Analyses isotopiques à haute précision de l'air piégé dans les glaces polaires pour la quantification des variations rapides de température: méthodes et limites, Notes des activités instrumentales de l'IPSL, 39, 2003.

Landais, A., Dreyfus, G., Capron, E., Masson-Delmotte, V., Sanchez-Goñi, M. F., Desprat, S., Hoffmann, G., Jouzel, J., Leuenberger, M., and Johnsen, S.: What drives the millennial and orbital variations of $\delta^{18}O_{atm}$?, Quaternary Sci. Rev., 29, 235–246, doi:10.1016/j.quascirev.2009.07.005, 2010.

Landais, A., Dreyfus, G. B., Capron, E., Jouzel, J., Masson-Delmotte, V., Roche, D. M., Prié, F., Caillon, N., Chappellaz, J., Leuenberger, M., Lourantou, A., Parrenin, F., Raynaud, D., and Teste, G.: EPICA Dome C Ice Core Terminations I and II Air Isotopes and CO_2 Data, NOAA/WDS for Paleoclimatology, https://www.ncei.noaa.gov/pub/data/paleo/icecore/antarctica/epica_domec/edc2013d18oatm.txt, 2013.

Landais, A., Masson-Delmotte, V., Stenni, B., Selmo, E., Roche, D.M., Jouzel, J., Lambert, F., Guillevic, M., Bazin, L., Arzel, O., Vinther, B., Gkinis, V., and Popp, T.: A review of the bipolar see–saw from synchronized and high resolution ice core water stable isotope records from Greenland and East Antarctica, Quaternary Sci. Rev., 114, 18−32, https://doi.org/10.1016/j.quascirev.2015.01.031, 2015.

Lisiecki, L. E. and Raymo, M. E.: A Pliocene-Pleistocene stack of 57 globally distributed benthic $\delta^{18}O$ records, Paleoceanography, 20, PA1003, https://doi.org/10.1029/2004pa001071, 2005.

Loosli, H. H., and Oeschger, H.: ^{37}Ar and ^{81}Kr in the atmosphere, Earth Planet Sc. Lett., 7, 67–71, https://doi.org/10.1016/0012-821X(69)90014-4, 1969.

Lourantou, A., Chappellaz, J., Barnola J.-M., Masson-Delmotte, V., and Raynaud, D.: Changes in atmospheric CO_2 and its carbon isotopic ratio during the penultimate deglaciation, Quaternary Sci. Rev., 29, 1983–1992, https://doi.org/10.1016/j.quascirev.2010.05.002, 2010.

Lu, Z.-T., Schlosser, P., Smethie Jr., W. M., Sturchio, N. C., Fischer, T. P., Kennedy, B. M., Purtschert, R., Severinghaus, J. P., Solomon, D. K., Tanhua, T., and Yokochi, R.: Tracer applications of noble gas radionuclides in the geosciences, Earth-

670   Sci. Rev., 138, 196–214, https://doi.org/10.1016/j.earscirev.2013.09.002, 2014.

Marcott, S. A., Bauska, T. K., Buizert, C., Steig, E. J., Rosen, J. L., Cuffey, K. M., Fudge, T. J., Severinghaus, J. P., Ahn, J., Kalk, M. L., McConnell, J. R., Sowers, T., Taylor K. C., White, J. W. C., and Brook, E. J.: Centennial-scale changes in the global carbon cycle during the last deglaciation, Nature, 514, 616–619, https://doi.org/10.1038/nature13799, 2014.

Menking, J. A., Brook, E. J., Shackleton, S. A., Severinghaus, J. P., Dyonisius, M. N., Petrenko, V., McConnell, J. R., Rhodes,

675   R. H., Bauska, T. K., Baggenstos, D., Marcott, S., and Barker, S.: Spatial pattern of accumulation at Taylor Dome during Marine Isotope Stage 4: stratigraphic constrains from Taylor Glacier, Clim. Past, 15, 1537–1556, https://doi.org/10.5194/cp-15-1537-2019, 2019.

Monnin, E., Indermühle, A., Dällenbach, A., Flückiger, J., Stauffer, B., Stocker, T. F., Raynaud, D., and Barnola, J.-M.: Atmospheric CO_2 concentrations over the last glacial termination, Science, 291, 112–114, DOI:

680   10.1126/science.291.5501.112, 2001.

Monnin, E., Steig, E. J., Siegenthaler, U., Kawamura, K., Schwander, J., Stauffer, B., Stocker, T. F., Morse, D. L., Barnola, J.-M., Bellier, B., Raynaud, D., Fischer, H.: Evidence for substantial accumulation rate variability in Antarctica during the Holocene, through synchronization of CO_2 in the Taylor Dome, Dome C and DML ice cores, Earth Planet Sc. Lett., 224, 45–54, https://doi.org/10.1016/j.epsl.2004.05.007, 2004.

685 Mouginot, J., Scheuchl, B., and Rignot, E.: Mapping of Ice Motion in Antarctica Using Synthetic-Aperture Radar Data, Remote Sensing, 4, 2753–2767, doi:10.3390/rs4092753, 2012.

Nakawo, M., Nagoshi, M., and Mae S.: Stratigraphic record of an ice core from the Yamato meteorite ice field, Antarctica, Ann. Glaciol., 10, 126–129, https://doi.org/10.3189/S0260305500004298, 1988.

Oeschger, H.: Accelerator mass spectrometry and ice core research, Nucl. Instrum. Meth. B., 29, 196–202,

690   https://doi.org/10.1016/0168-583X(87)90235-7, 1987.

Oyabu, I., Kawamura, K., Kitamura, K., Dallmayr, R., Kitamura, A., Sawada, C., Severinghaus, J. P., Beaudette, R., Orsi, A., Sugawara, S., Ishidoya, S., Dahl-Jensen, D., Goto-Azuma, K., Aoki, S., and Nakazawa, T.: New technique for high-precision, simultaneous measurements of CH_4, N_2O and CO_2 concentrations; isotopic and elemental ratios of N_2, O_2 and Ar; and total air content in ice cores by wet extraction, Atmos. Meas. Tech., 13, 6703–6731, https://doi.org/10.5194/amt-

695   13-6703-2020, 2020.

Petit, J.R., Jouzel, J., Raynaud, D., Barkov, N. I., Barnola, J.-M., Basile, I., Bender, M., Chappellaz, J., Davis, M., Delaygue, G. Delmotte, M., Kotlyakov, V. M., Legrand, M., Lipenkov, V. Y., Lorius, C., PÉpin, L., Ritz, C., Saltzman, E., and Stievenard, M.: Climate and atmospheric history of the past 420,000 years from the Vostok ice core, Antarctica, Nature, 399, 429–436, https://doi.org/10.1038/20859, 1999.

700   Petrenko, V. V., Severinghaus, J. P., Brook, E. J., Reeh, N., and Schaefer, H.: Gas records from the West Greenland ice margin covering the Last Glacial Termination: a horizontal ice core, Quaternary Sci. Rev., 25, 865–875, https://doi.org/10.1016/j.quascirev.2005.09.005, 2006.

Reeh, N., Oerter, H., Letréguilly, A., Miller, H., and Hubberten, H.-W.: A new, detailed ice-age oxygen-18 record from the ice-sheet margin in central West Greenland, Global. Planet. Change, 4, 373–383, https://doi.org/10.1016/0921-
705   8181(91)90003-F, 1991.

Reeh, N., Oerter, H., and Thomsen, H. H.: Comparison between Greenland ice-margin and ice-core oxygen-18 records, Ann. Glaciol., 35, 136–144, https://doi.org/10.3189/172756402781817365, 2002.

Reynolds, J. M.: Dielectric Behaviour of Firn and Ice from the Antarctic Peninsula, Antarctica, J. Glaciol., 31, 253–262, doi:10.3189/S0022143000006584, 1985.

710   Rhodes, R. H., Brook, E. J., Blunier, T., McConnell, J. R., and Romanini, D.: Experiment-time-integrated CH_4 data from all 3 instruments, calibrated and corrected for solubility and gravitational effects of the WAIS-Divide ice core, Antarctica, PANGAEA, https://doi.org/10.1594/PANGAEA.875980, 2017.

Rignot, E., Mouginot, J., and Scheuchl, B.: Ice Flow of the Antarctic Ice Sheet, Science, 333, 1427–1430, DOI: 10.1126/science.1208336, 2011.

715   Schaefer, H., Whiticar, M. J., Brook, E. J., Petrenko, V. V., Ferretti, D. F., and Severinghaus J. P.: Ice record of $\delta^{13}C$ for atmospheric CH_4 across the Younger Dryas-Preboreal transition, Science, 313, 1109–1112, DOI: 10.1126/science.1126562, 2006.

Schaefer, H., Petrenko, V. V., Brook, E. J., Severinghaus, J. P., Reeh, N., Melton, J. R., and Mitchell, L.: Ice stratigraphy at the Pâkitsoq ice margin, West Greenland, derived from gas records, J. Glaciol., 55, 411–421,
720   doi:10.3189/002214309788816704, 2009.

Schmitt, J., Schneider, R., Elsig, J., Leuenberger, D., Lourantou, A., Chappellaz, J., Köhler, P., Joos, F., Stocker, T. F., Leuenberger, M., and Fischer, H.: Carbon isotope constraints on the deglacial CO_2 rise from ice cores, Science, 336, 711–714, DOI: 10.1126/science.1217161, 2012.

Schwander, J., and Stauffer, B.: Age difference between polar ice and the air trapped in its bubbles, Nature, 311, 45–47,
725   https://doi.org/10.1038/311045a0, 1984.

Schwander, J., Sowers, T., Barnola, J.-M., Blunier, T., Fuchs, A., and Malaizé B.: Age scale of the air in the summit ice: Implication for glacial-interglacial temperature change, J. Geophys. Res., 102, 19483–19493, https://doi.org/10.1029/97JD01309, 1997.

Seltzer, A. M., Buizert, C., Baggenstos, D., Brook, E. J., Ahn, J., Yang, J.-W., and Severinghaus, J. P.: Does $\delta^{18}O$ of O_2 record
730   meridional shifts in tropical rainfall?, Clim. Past, 13, 1323–1338, https://doi.org/10.5194/cp-13-1323-2017, 2017.

Severi, M., Udisti, R., Becagli, S., Stenni, B., and Traversi, R.: Volcanic synchronisation of the EPICA-DC and TALDICE ice cores for the last 42 kyr BP, Clim. Past, 8, 509–517, https://doi.org/10.5194/cp-8-509-2012, 2012.

Severinghaus, J. P., Sowers, T., Brook, E. J., Alley, R. B., and Bender, M. L.: Timing of abrupt climate change at the end of the Younger Dryas interval from thermally fractionated gases in polar ice, Nature, 391, 141–146,
735   https://doi.org/10.1038/34346, 1998.

Severinghaus, J. P., Beaudette, R., Headly, M. A., Taylor, K., and Brook, E. J.: Oxygen-18 of O_2 Records the Impact of Abrupt Climate Change on the Terrestrial Biosphere, Science, 324, 1431–1434, DOI: 10.1126/science.1169473, 2009.

Severinghaus, J. P.: Low-res d15N and d18O of O2 in the WAIS Divide 06A Deep Core, U.S. Antarctic Program (USAP) Data Center, doi: https://doi.org/10.7265/N5S46PWD, 2015.

740   Shin, J.: Atmospheric CO_2 variations on millennial time scales during the early Holocene, M.S. thesis, School of Earth and Environmental Sciences, Seoul National University, South Korea, 2014.

Siegenthaler, U., Stocker, T. F., Monnin, E., Lüthi, D., Schwander, J., Staffer, B., Raynaud, D., Barnola, J.-M., Fischer, H., Masson-Delmotte, V., and Jouzel, J.: Stable carbon cycle–climate relationship during the late Pleistocene, Science, 310, 1313–1317, DOI: 10.1126/science.1120130, 2005.

745   Sigl, M., Fudge, T. J., Winstrup, M., Cole-Dai, J., Ferris, D., McConnell, J. R., Taylor, K. C., Welten, K. C., Woodruff, T. E., Adolphi, F., Bisiaux, M., Brook, E. J., Buizert, C., Caffee, M. W., Dunbar, N. W., Edwards, R., Geng, L., Iverson, N., Koffman, B., Layman, L., Maselli, O. J., McGwire, K., Muscheler, R., Nishiizumi, K., Pasteris, D. R., Rhodes, R. H., and Sowers, T. A.: The WAIS Divide deep ice core WD2014 chronology – Part 2: Annual-layer counting (0–31 ka BP), Clim. Past, 12, 769–786, https://doi.org/10.5194/cp-12-769-2016, 2016.

750   Sinisalo, A., Grinsted, A., Moore, J., Meijer, H., Martma, T., and Van De Wal, R. S. W.: Inferences from stable water isotopes on the Holocene evolution of Scharffenbergbotnen blue-ice area, East Antarctica, J. Glaciol., 53, 427–434, https://doi.org/10.3189/002214307783258495, 2007.

Sinisalo, A. and Moore, J. C.: Antarctic blue ice area – towards extracting palaeoclimate information, Antarct. Sci., 22, 99–115, https://doi.org/10.1017/S0954102009990691, 2010.

755   Sowers, T., Bender, M., Labeyrie, L., Martinson, D., Jouzel, J., Raynaud, D., Pichon, J. J., and Korotkevich, Y. S.: A 135,000-year Vostok-Sepcmap Common temporal framework, Paleoceanography, 8, 737–766, https://doi.org/10.1029/93PA02328, 1993.

Spaulding, N. E., Higgins, J. A., Kurbatov, A. V., Bender, M. L., Arcone, S. A., Campbell, S., Dunbar, N. W., Chimiak, L. M., Introne, D. S., and Mayewski, P. A.: Climate archives from 90 to 250 ka in horizontal and vertical ice cores from the Allan
760   Hills Blue Ice Area, Antarctica, Quaternary Res., 80, 562–574, https://doi.org/10.1016/j.yqres.2013.07.004, 2013.

Steffensen, J. P., Andersen, K. K., Bigler, M., Clausen, H. B., Dahl-Jensen, D., Fischer, H., Goto-Azuma, K., Hansson, M., Johnsen, S. J., Jouzel, J., Masson-Delmotte, V., Popp, T., Rasmussen, S. O., Röthlisberger, R., Ruth, U., Stauffer, B., Siggaard-Andersen, M.-L., Sveinbjörnsdóttir, Á. E., Svensson, A., and White, J. W. C.: High-resolution Greenland ice core data show abrupt climate change happens in few years, Science, 321, 680–684, DOI: 10.1126/science.1157707, 2008.

765   Stenni, B., Buiron, D., Frezzotti, M., Albani, S., Barbante, C., Bard, E., Barnola, J. M., Baroni, M., Baumgartner, M., Bonazza, M., Capron, E., Castellano, E., Chappellaz, J., Delmonte, B., Falourd, S., Genoni, L., Iacumin, P., Jouzel, J., Kipfstuhl, S.,

Landais, A., Lemieux-Dudon, B., Maggi, V., Masson-Delmotte, V., Mazzola, C., Minster, B., Montagnat, M., Mulvaney, R., Narcisi, B., Oerter, H., Parrenin, F., Petit, J. R., Ritz, C., Scarchilli, C., Schilt, A., Schüpbach, S., Schwander, J., Selmo, E., Severi, M., Stocker, T. F., and Udisti, R.: Expression of the bipolar see-saw in Antarctic climate records during the last

770   deglaciation, Nat. Geosci., 4, 46–49, https://doi.org/10.1038/ngeo1026, 2010.

Tian, L., Ritterbusch, F., Gu J.-Q., Hu, S.-M., Jiang, W., Lu, Z.-T., Wang, D., and Yang, G.-M.: [81]Kr Dating at the Guliya Ice Cap, Tibetan Plateau, Geohys. Res. Lett., 46, 6636–6643, https://doi.org/10.1029/2019GL082464, 2019.

Turney, C., Fogwill, C., Van Ommen, T. D., Moy, A. D., Etheridge, D., Rubino, M., Curran, M. A. J., and Rivera, A.: Late Pleistocene and early Holocene change in the Weddell Sea: a new climate record from the Patriot Hills, Ellsworth

775   Mountains, West Antarctica, J. Quaternary Sci., 28, 697–704, https://doi.org/10.1002/jqs.2668, 2013.

Welten, K. C., Folco, L., Nishiizumi, K., Caffee, M. W., Grimberg, A., Meier, M. M. M., and Kober, F.: Meteoritic and bedrock constraints on the glacial history of Frontier Mountain in northern Victoria Land, Antarctica, Earth Planet. Sc. Lett., 270, 308–315, https://doi.org/10.1016/j.epsl.2008.03.052, 2008.

Whillans, I. M. and Cassidy, W. A.: Catch a falling star: Meteorites and old ice, Science, 222, 55–57, DOI:

780   10.1126/science.222.4619.55, 1983.

Yan, Y., Bender, M. L., Brook, E. J., Clifford, H. M., Kemeny, P. C., Kurbatov, A. V., Mackay, S., Mayewski, P. A., Ng, J., Severinghaus J. P., and Higgins, J. A.: Two-million-year-old snapshots of atmospheric gases from Antarctic ice, Nature, 574, 663–666, https://doi.org/10.1038/s41586-019-1692-3, 2019.

Yang, J.-W.: Paleoclimate reconstruction from greenhouse gas and borehole temperature of polar ice cores, and study on the

785   origin of greenhouse gas in permafrost ice wedges, Ph.D. thesis, School of Earth and Environmental Sciences, Seoul National University, South Korea, 2019.

Yau A. M., Bender, M. L., Marchant, D. R., and Mackay, S. L.: Geochemical analyses of air from an ancient debris-covered glacier, Antarctica, Quat. Geochronol., 28, 29–39, https://doi.org/10.1016/j.quageo.2015.03.008, 2015.

Zappala, J. C., Baggenstos, D., Gerber, C., Jiang, W., Kennedy, B. M., Lu, Z.-T., Masarik, J., Mueller, P., Purtschert, R., and

790   Visser, A.: Atmospheric [81]Kr as an Integrator of Cosmic-Ray Flux on the Hundred-Thousand-Year Time Scale, Geophys. Res. Lett., 47, https://doi.org/10.1029/2019GL086381, 2020.